The Joined Wing: An Overview

Julian Wolkovitch
ACA Industries, Inc., Torrance, California

Nomenclature

A = aspect ratio, b^2/S
B = span ratio (rear wing/front wing)
b = span
b' = effective span (see Sec. II)
C = chord ratio (rear wing/front wing)
C_D = drag coefficient, drag/qS
C_L = lift coefficient, lift/qS
C_m = moment coefficient, pitching moment/$qS\bar{c}$
C_n = yawing moment/qSb
C_l = rolling moment/qSb
$\bar{c}$ = reference chord
d' = effective beam depth (see Sec. II)
e = span-efficiency factor
GPA = gross projected area of all lifting surfaces on a plane containing the aircraft longitudinal axis and normal to the airplane's plane of symmetry
L = lift
n = load factor
q = dynamic pressure
S = reference area
W = gross weight
W_w = wing weight
α = angle of attack
β = sideslip angle
Γ = dihedral angle
ϵ = downwash angle
Λ = sweep angle of quarter-chord line
λ = taper ratio (tip chord/root chord)

Subscripts
F = front wing
R = rear wing

I. Introduction

THE joined-wing airplane may be defined as an airplane that incorporates tandem wings arranged to form diamond shapes in both plan and front views.[1-3] This general concept can take different forms, as shown in Figs. 1-4, which show joined-wing tunnel models. All the models obtain the desired diamond-shaped front view by locating the root of the rear wing at or near the top of the vertical tail(s). Figure 1 shows a transonic model[4] having wings joined by means of streamlined tip bodies. Figure 2 shows a wind tunnel model that combines a joined wing with a 60-deg sweep canard.[5] In both the configurations shown in Figs. 1 and 2, the wing-joining members are small bodies, but it is also possible to join the wings by lifting surfaces (winglets) as shown in Fig. 3. This configuration uses twin fins to support the center section of the rear wing. The interwing joint may also be located inboard of the tips as shown in Fig. 4; this shows a wind tunnel model of a design for an agricultural airplane.[6] In this design the pilot is located in the vertical tail, which has an airfoil of 18% thickness/chord ratio. Other joined-wing arrangements are possible, as described in Refs. 1-3.

Advantages claimed for the joined wing include:
1) Light weight.
2) High stiffness.
3) Low induced drag.
4) Good transonic area distribution.
5) High trimmed C_L max.
6) Reduced wetted area and parasite drag.
7) Direct lift control capability.
8) Direct sideforce control capability.
9) Good stability and control.

These claims have been supported by independent analyses, design studies and wind tunnel tests, as described later.

Joined wings differ from conventional wings in their internal structure as well as their external configuration. This important difference is illustrated in Figs. 5 and 6. Figure 5 shows how the lift loads acting on each wing can be resolved into components acting normal and parallel to the truss structure formed by the joined wings. The in-plane components are well resisted by the truss structure. The out-of-plane components tend to bend the wings about a tilted bending axis, as shown in Fig. 5. To resist this, the wing structural material must form a deep spar about this axis. This implies that the material must be concentrated near the upper leading edge and lower trailing edge, as shown in the lower portion of Fig. 5.

The above arrangement is different from that of a cantilever wing. Figure 6 portrays schematically a section of a typical subsonic transport wing. The lift loads on the wing are resisted by a box beam extending from typically 15% to 65% of the chord. The box beam also serves as a fuel tank. Over most of the span, the box beam employs upper and lower skins which,

---

Dr. Wolkovitch received his B.S., M.S., and Ph.D. degrees in Aeronautical Engineering from the University of London. Since 1954 he has been engaged in design and research in aerodynamics and control systems of airplanes, missiles, and helicopters. Initially he was employed by Folland Aircraft Ltd. in England. After immigrating to the U.S. in 1958, he joined the Convair Division of General Dynamics Corporation. Subsequently he was employed by Systems Technology Inc., Mechanics Research Inc., and Vought Corporation. Since 1982 he has been President of ACA Industries, Inc., a small research and consulting company. Much of his recent effort has been devoted to the joined wing, including research studies for the U.S. Navy, NASA, and other government agencies, and consulting for airframe manufacturers. He has authored numerous technical papers, and was awarded the Wright Brothers Medal of the Society of Automotive Engineers.

Presented as Paper 85-0274 at the AIAA 23rd Aerospace Sciences Meeting, Reno, NV, Jan. 14-17, 1985; received Jan. 29, 1985; revision received Oct. 18, 1985.

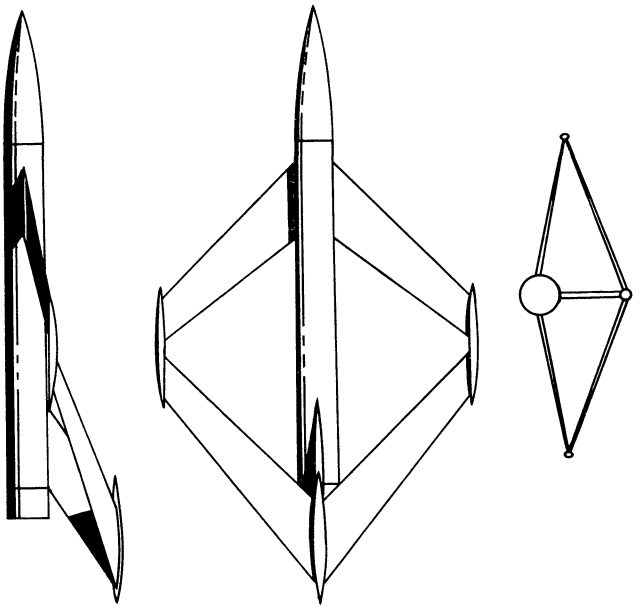

Fig. 1 Rockwell transonic wind tunnel model.

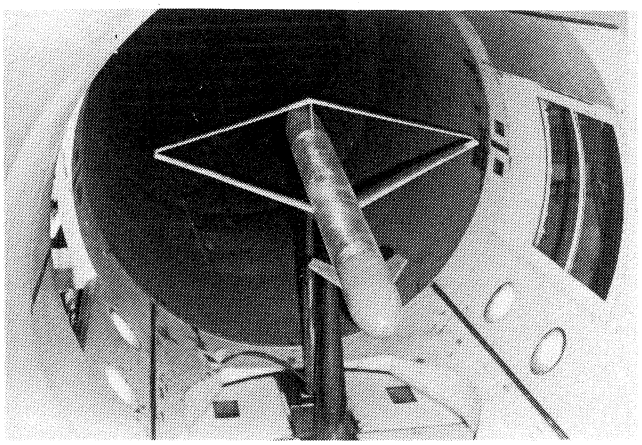

Fig.2 Joined-wing wind tunnel model with 60-deg sweep canard.

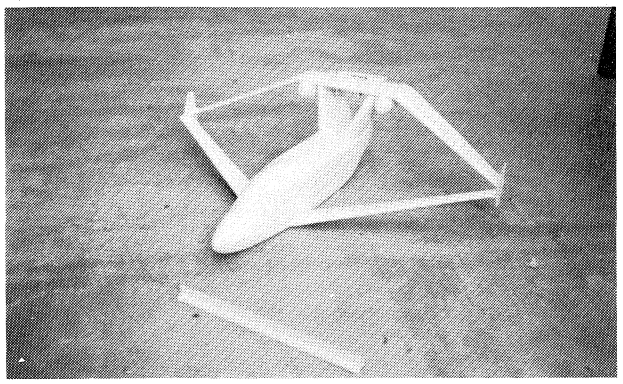

Fig. 3 University of Kansas wind tunnel model with twin fins and winglets.

at a given spanwise station, are of relatively constant thickness across the chord of the beam. This is expected because the maximum bending strength for a given weight of structural material is obtained by maximizing the second moment of area of the beam about its bending axis. Hence, it is not profitable to extend the structural box forward of 15% or aft of 65% of the airfoil chord since in these regions the airfoil thickness (beam depth) is less than in the midportion of the airfoil.

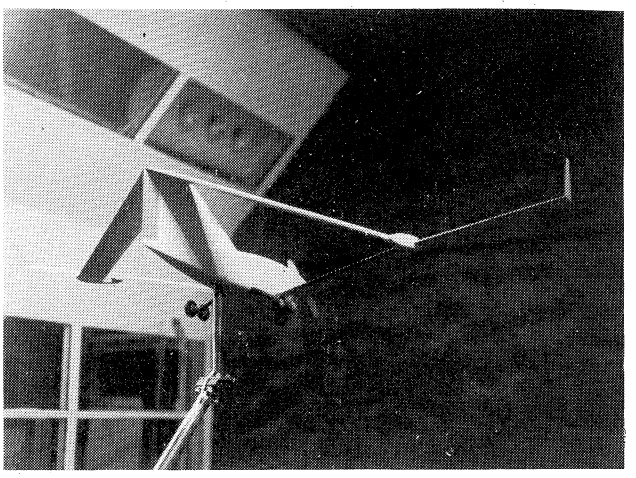

Fig. 4 NASA wind tunnel model of agricultural airplane design.

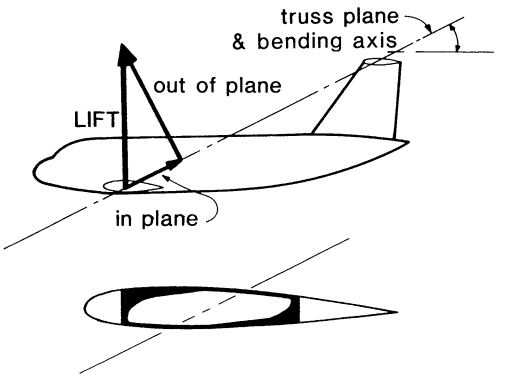

Fig. 5 Tilted bending axis of a joined wing.

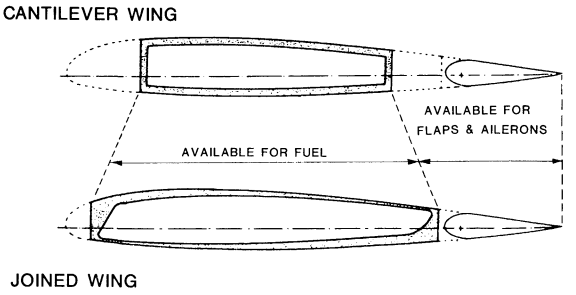

Fig. 6 Optimum wing structures.

As explained above and in Refs. 1,3, and 7, the joined wing's strength/weight ratio is maximized by concentrating the bending-resistant material near the upper leading edges and lower trailing edges. Consequently, an optimum joined-wing structure occupies large percentages of the chords of its airfoils. For both the front and rear wings, the structural box may extend from the leading edge to the trailing edge of the fixed part of the airfoil. The limits are set by the space needed for deicing systems, flaps, high-lift devices, and actuators. The effective beam depth of a joined wing is primarily determined by the chord of its airfoils; their thickness is secondary. Hence, thin airfoils may be employed with less weight penalty than for cantilever wings.

Finite element structural analyses[7] confirm that, except in certain limited regions (e.g., near the interwing joint), the optimum material distribution conforms to the above simple model.

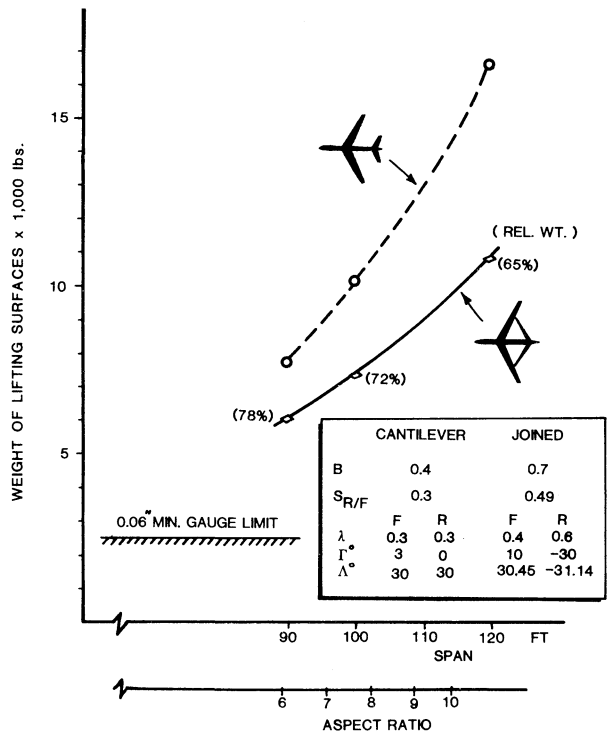

Fig. 7 Weight of lifting surfaces of turboprop transports vs aspect ratio.

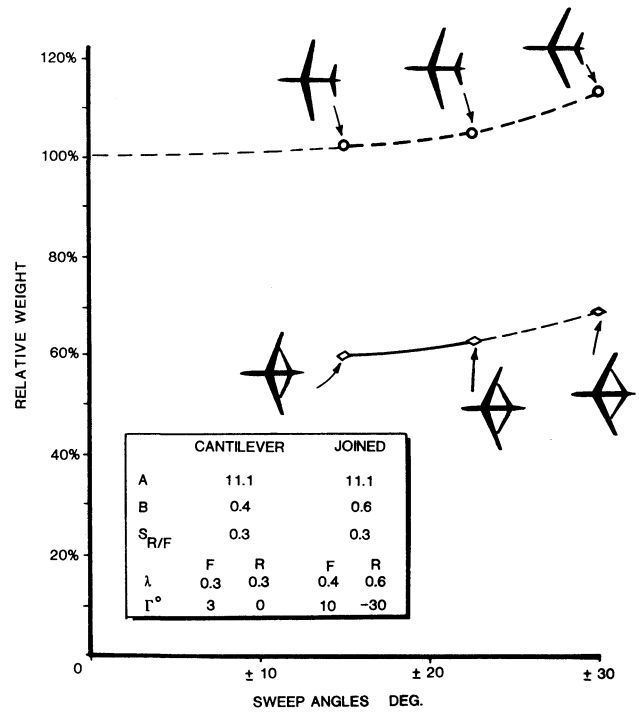

Fig. 8 Effect of sweep on relative weight of lifting surfaces of turboprop transports.

Organization of This Paper

It is important to understand that the joined wing is a highly integrated concept that links structural and aerodynamic features in novel ways. The present paper, therefore, first outlines the structural principles of the joined wing (in Sec. II). These principles must be understood in order to effectively perform joined-wing aerodynamic design, which is discussed in Sec. III. Stability and control aspects of joined wings are examined in Sec. IV. The close interaction of joined-wing structural and aerodynamic characteristics provides some novel problems of configuration design, which are discussed in Sec. V. Specific designs, projects, and concepts employing joined wings are presented in Sec. VI, together with a brief assessment of the performance benefits of the joined wing. Conclusions are given in Sec. VII, which is followed by an Appendix giving historical and technical information on other aircraft configurations related to the joined wing.

II. Results of Structural Analyses

Weight Comparisons

Shyu and Miura, of NASA Ames Research Center, have performed comprehensive structural analyses of joined wings, employing the EAL, SPAR, and NASTRAN finite element programs.[8] Reference 10 compares their results with the results obtained independently by Samuels[7] and Hajela,[11] who employed the SAP-5 and ACCESS-3 finite element programs, respectively. Reference 10 shows that the results obtained by Shyu and Miura are consistent with those of Samuels and Hajela.

By analyzing wider ranges of geometric parameters than were studied by Samuels or Hajela, Shyu and Miura found some joined-wing configurations that gave large weight savings. For example, Fig. 7 shows results of Refs. 8 and 9 showing the effect of sweep on the weights of transport wings. This figure compares the weights of joined vs conventional wing-plus-tail systems that are aerodynamically equivalent. That is, both systems have the same gross projected areas, equal taper ratios, equal magnitudes of sweep angles (sweepback for the wing and tail, sweepback and sweepforward for the joined wing), and equal ratios of front to rear lifting surface projected areas. The total design airloads and the structural material properties were also made equal in these comparisons, which employed identical optimization techniques. A streamwise thickness/chord ratio of 12% was employed for all lifting surfaces. Figure 7 shows that the joined wing typically weighs 65 to 78% of the weight of the aerodynamically equivalent cantilever wing-plus-tail. (The above comparison and the others cited here include all the nonmovable portions of the wing, including the interwing joint. Control surface weights are not included for either the joined or conventional configurations and are approximately equal for both types of wing systems.)

The above comparison did not exactly achieve the condition for aerodynamic equivalence since the quarter-chord sweep angles of the joined wing (30.45, −31.14 deg) were slightly larger than those of the cantilever wing and tail (30 deg on each surface). The relative advantage of the joined wing improves as sweep is reduced. This is shown in Fig. 8, which graphs further results of Shyu and Miura.[8,9] Figure 8 compares the weights of aerodynamically equivalent systems constructed from aluminum and employing a streamwise thickness/chord ratio of 12.0%. The relative weights are graphed vs the magnitude of the sweep angle employed on each lifting surface (positive and negative for the joined wing, positive for the conventional system). At least one surface of the joined wing must be swept, whereas the cantilever wing and tail can both be unswept. Nevertheless, the joined wing shows a large weight saving at all sweep angles. For example, at 15 deg sweep the joined wing weighs only 58% of the 15-deg sweep wing-plus-tail and approximately 60% of the unswept cantilever system.

Joined wings are not invariably lighter than aerodynamically equivalent conventional wing-plus-tail systems. Weight will be saved only if:

1) The geometric parameters of the joined wing such as sweep, dihedral, taper ratio, and joint location (as a fraction of the span) are properly chosen.

2) The internal wing structure is optimized, with the wing box occupying the section of the airfoil between 5 and 75% chord (or greater if possible).

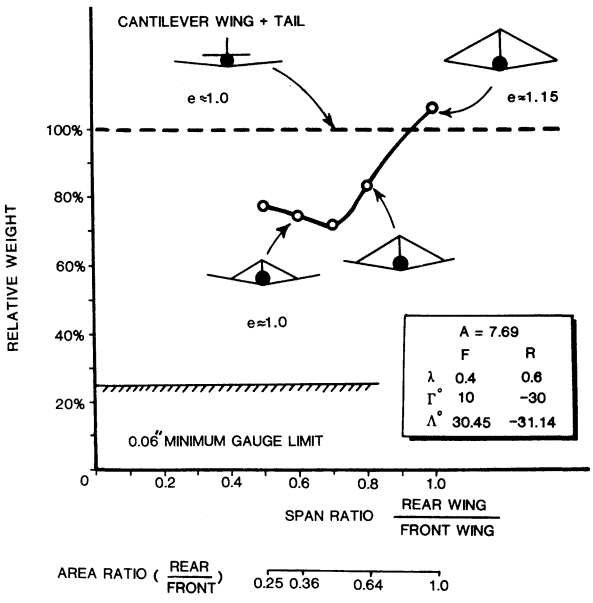

Fig. 9 Effect of span ratio on relative weight and span-efficiency factor.

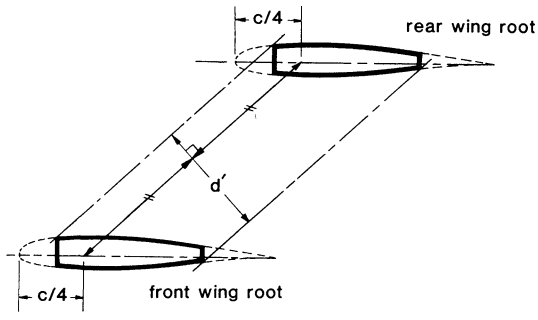

Fig. 10 Effective beam depth parameter.

Guidance on the selection of the geometric parameters for minimum weight is given below.

Effect of Joint Location

For a given span, GPA, and maximum lift, with constant sweep and dihedral angles, locating the interwing joint inboard provides a lighter wing system than joining the wings at their tips. However, the tip-jointed arrangement has some aerodynamic advantages (such as higher span-efficiency factor, suitability for winglets, and greater trimming moment capability). In general, joint locations of from 60-100% of the span must be considered to arrive at an overall optimum design.

The above considerations are illustrated in Fig. 9, which graphs results of Refs. 8 and 9 on the effect of span ratio on weight. Figure 9 shows that, for the particular taper ratios considered (0.3 for the cantilever surfaces, 0.4 and 0.6 respectively, for the front and rear joined wings), the lightest joined wing is obtained with a span ratio of 0.7, i.e., the tip of the rear wing structure connects to the front wing structure at 0.70 of the span of the front wing. Figure 9 also shows that the tip-jointed configuration is heavier than the cantilever system of the same span. Therefore, it might be thought that the tip-jointed configuration need not be considered further. However, this would not be correct: as noted in Fig. 9, the tip-jointed configuration has a span-efficiency factor e, which (as discussed later) is substantially higher than that of the inboard-jointed configuration or that of the cantilever configuration. Thus, to obtain true aerodynamic equivalence, the span of the tip-jointed joined-wing configuration should be reduced to give the same induced drag (at equal weight and speed) as the conventional configuration. If this is done, and if higher taper (taper ratio = 0.3) is employed on both the front and rear wings, it is found that the tip-jointed configuration weighs approximately 80% of the weight of the cantilever wing-plus-tail. This is still higher than the optimum achieved by the configuration having the wings joined at 70% span. However, the weight advantage of the latter is not so great that it could not be overriden by aerodynamic advantages of the tip-jointed configuration, such as higher trimming moments or suitability for winglets. This example emphasizes the need to consider several joint locations in determining an overall optimum design and to integrate structural and aerodynamic considerations.

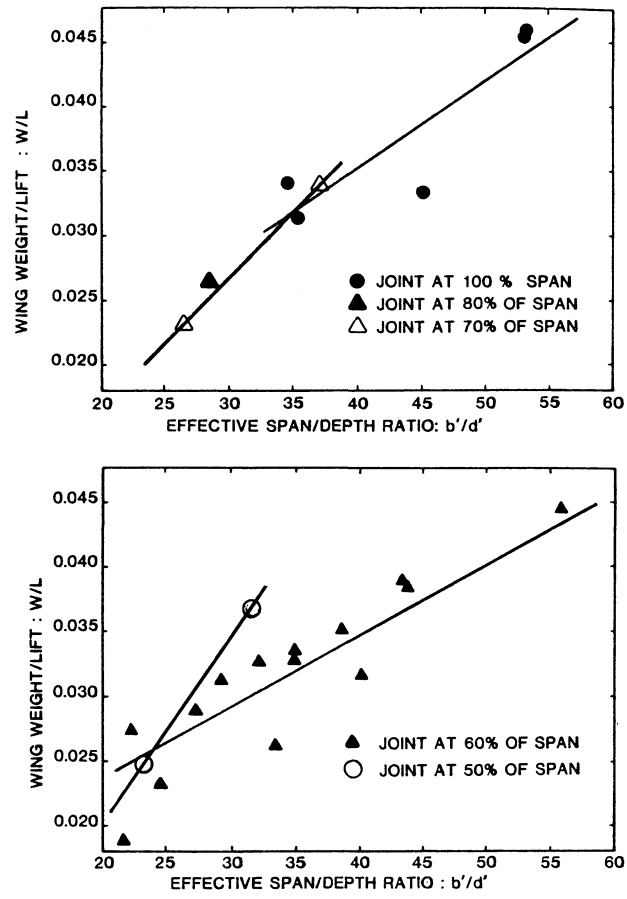

Fig. 11 Correlations of computed weights vs effective (depth/span) ratio parameter.

Weight Prediction

For conventional wings, weight data are frequently correlated in terms of span, maximum root chord thickness, and other geometric parameters, as well as material properties. Reference 10 shows that similar correlations can be produced for joined wings using two parameters denoted as effective depth (d') and effective span (b'). The effective depth parameter is defined from the root centerline chords of the front and rear wings as shown in Fig. 10. The effective span is defined as the mean of the true (not projected) lengths of the quarter-chord lines of the front and rear wings and is given by

$$b' = 0.5[(b_F/\cos\Gamma_F\cos\Lambda_F) + (b_R/\cos\Gamma_R\cos\Lambda_R)]$$

The ratio of b' to d' will be referred to as the effective span/depth.

Figure 11 shows the results of correlating W_W/L, $(= W_W/nW)$, wing system weight/lift with the effective

span/depth for the joined wings considered in Ref. 8. These included variations of the parameters in Table 1.

The correlations of Fig. 11 show that the weight is minimized by decreasing the effective span/depth ratio. This requires: 1) Large dihedral (positive and negative), 2) Low sweep angles (positive and negative), and 3) High taper ratios (front and rear).

Reference 8 shows that the sensitivity of weight to the thickness/chord ratio is typically 30% less for joined wings than for cantilever wings. Joined wings are therefore particularly suitable for thin airfoils.

Special Structural Characteristics

Column Buckling Considerations

Under positive load factors, the rear wing of a joined-wing pair is in compression. Therefore, overall column buckling must be considered. In the work of Shyu and Hajela reported above, buckling was checked using the "differential stiffness" option of NASTRAN. Buckling was not found to be a constraint. The minimum wing thickness/chord ratio employed was 0.12; thinner wings would be more prone to exhibit column buckling phenomena. To avoid this, pin-joints with horizontal axes should not be used on joined wings. For ultrathin wings minimum weight may be obtained by employing a strut linking the leading edge of the rear wing to the trailing edge of the front wing. The column length of the rear wing can also be reduced by employing twin fins, as in Fig. 3, and/or an inboard location for the interwing joint.

The torsional stiffness of joined wings is high since torsion of one wing is resisted by flexure of the other (see Fig. 12). This leads to higher aileron effectiveness than is obtainable with cantilever wings of comparable weight. It also yields higher flutter speeds, as described below.

Aeroelasticity

Aeroelastic characteristics of joined wings have been studied by theoretical analyses[7,12] and also by tests performed on flutter models.[13] These tests were performed in the NASA Langley Research Center variable density transonic dynamics tunnel. Half-models of high-altitude RPV wing concepts were tested, comparing joined vs cantilever wings of equal span, weight, and GPA. Figure 13 shows the joined-wing model. The aspect ratios of the models were high ($A=21.6$ for both models, giving $A=43.2$ for each individual joined wing). The tests were performed at $M=0.4$ and 0.6. At each Mach number, the dynamic pressure for aeroelastic instability (q') was found to be approximately 1.6 times the value of q' for the cantilever wing. It should be noted that the internal structure of the joined-wing model did not employ the optimum leading-edge/trailing-edge (L.E./T.E.) spar arrangement of Fig. 6. Instead, a single spar was used, located at approximately 40% chord. It is possible that still better results would have been obtained if the spar arrangement had been optimized.

Other aeroelastic analyses of joined wings have been performed, e.g., Ref. 12. This reference predicts large gains in flutter speed for the joined wing, but does not compare aerodynamically equivalent systems and apparently neglects the fore-and-aft degree of freedom of joined wings. This is significant and was included in the other references cited. In general, flutter analyses of joined wings should consider the effects of horizontal as well as vertical displacements of wing elements.

Fuselage Structural Weight and Stiffness

In general, under maximum positive load factor, the front and rear wings of a joined-wing pair both lift upward. Thus, the fuselage is supported near both ends: by contrast, a conventional wing-plus-tail system supports the fuselage near its middle, with the tail applying a trimming download. The net result is that the fuselage bending moments produced by a joined wing are smaller than those produced by a comparable wing-plus-tail. Lateral and torsional fuselage loads may also be reduced since the joined wing provides additional load paths to withstand rolling and yawing moments applied by gusts or by control surfaces. The savings in fuselage structural weight obtainable through the joined wing depend on the extent to which the fuselage is designed by pressurization loads as opposed to airloads. However, for many fuselages it would appear that significant weight can be saved, and this aspect of the joined wing deserves further study.

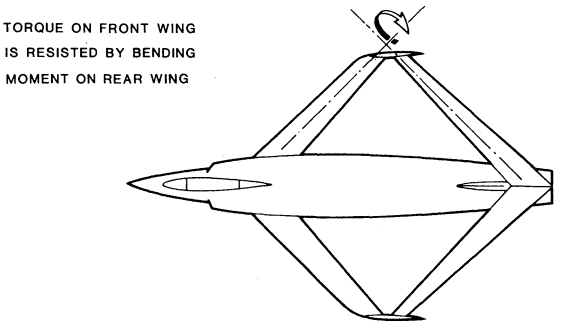

Fig. 12 Resistance of torsion of one wing by flexure of the other.

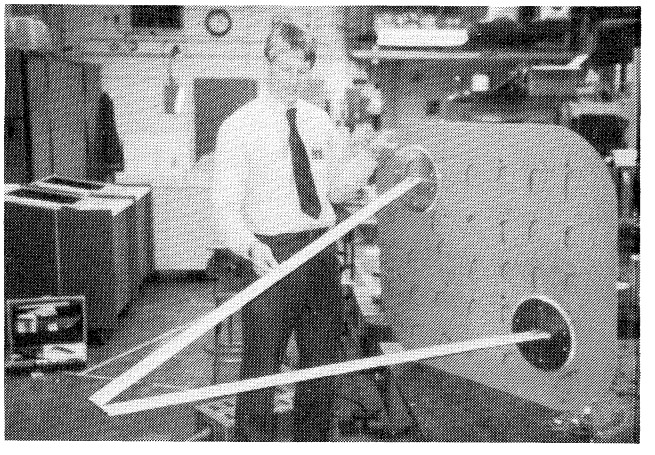

Fig. 13 NASA Langley joined-wing flutter model.

Table 1 Parameter variations for joined wing (Refs. 8 and 9)

Parameter	Min.	Max.
Aspect ratio, $A=b^2/\text{GPA}$	4.81	16.25
Span ratio, $B=b_R/b_F$	0.5	1.0
Area ratio, $B/C=S_R/S_F$	0.3	1.0
Taper ratio λ_F, λ_R	0.20, 0.25	0.75, 0.75
Sweep, Λ_F, Λ_R deg.	15.0-15.0	45.0-45.0
Dihedral Γ_F, Γ_R deg.	5.0-10.0	30.0-30.0
Thickness/chord ratio	0.12	0.15

Fin Structure

The fin must support symmetric and asymmetric loads transmitted via the rear wing root. This does not necessarily lead to a heavy fin structure because:

1) For a given overall sideslip angle, the total sideforce acting on the fin and wings is considerably less than would act on these components in isolation. This is due to the flow-straightening effect of each component on the others.

2) Due to the large anhedral of the rear wing, sideslip-induced rolling moments that it applies to the fin root op-

pose those due to fin sideforces. The rear wing also provides substantial inertia relief.

Twin fins having approximately 60-deg dihedral can be employed, as shown in Figs. 3 and 14. This arrangement reduces the unsupported column length of the rear wing and permits mounting the engines in the "armpit" formed by the fin and rear wing. In this location the engines are rigidly supported, and the pusher or tractor propellers produce little noise in the passenger cabin. The "armpit" mounting also eliminates some of the wetted area of the nacelles, fins, and rear wings. The twin-fin arrangement requires that the rear wing center section have little or no sweep and no dihedral. Since this portion of the wing is lightly loaded in cruise, these requirements may well be acceptable from an aerodynamic viewpoint.

Structure of Joined-Wing Wind Tunnel Models

The structural design of joined-wing wind tunnel models has been a recurring source of difficulty. The wings of wind tunnel models are typically machined from slabs of uniform (solid) material. Hence, they do not have the optimum concentration of structural material shown in Fig. 6. Relative to comparable "solid" cantilever wings, "solid" joined wings contain less volume of structural material, and it is not as well distributed to resist lift loads. The problem is compounded by the standard practice of using simple beam formulas to calculate stresses in wind tunnel models. This is adequate for cantilever wings but is not acceptable for joined wings. Any wind tunnel program involving joined wings must include adequate stress analyses by finite-element methods to check model safety and predict aeroelastic deflections.

III. Joined-Wing Aerodynamics

Induced Drag

This subsection presents results relating to induced drag computed by standard Prandtl-Munk biplane theory. This theory assumes that the vortex sheet shed by the front lifting surface remains undistorted (no roll-up) and parallel to the freestream (no downward drift). Munk[14] noted that the latter assumption overestimates the induced drag of back-staggered configurations because it overpredicts the downwash induced on the rear wing by the front wing. This error is of little consequence for the biplane configurations that were of interest to Prandtl and Munk because their stagger is small compared to their span. For joined-wing configurations, the stagger is large, and wind tunnel test data indicate that the span-efficiency factors computed by the Prandtl-Munk theory are too low. Accordingly, we first present the theoretical span-efficiency factors for various joined-wing configurations and then give correction factors based upon experimental data.

Figure 15 shows the span-efficiency factor e for optimally loaded joined wings with winglets inclined at 90 deg to the chord plane of each wing. Note that e may be expressed in terms of induced-drag coefficient, lift coefficient, and aspect ratio as

$$e = C_L^2/\pi A C_{D_i} \tag{1}$$

or in terms of induced drag, lift, and span as

$$e = L^2/\pi q b^2 D_i \tag{2}$$

The numerical value of e resulting from Eq. 2 is identical to that given by Eq. 1, but Eq. 2 has the advantage of showing that the value of e is independent of the choice of reference area.

Figure 15 is based upon theoretical analyses of Letcher[15] and Kuhlman.[16] Letcher obtained a solution for e for diamond-shaped wings without winglets; by Munk's stagger theorem this solution applies for all wings having the same Trefftz-plane configuration; hence, it includes tip-jointed joined wings. Letcher's analytic solution was subsequently verified by Kuhlman, using numerical optimization procedures. Kuhlman also showed that the optimal span-loading is almost elliptic for joined wings without winglets.

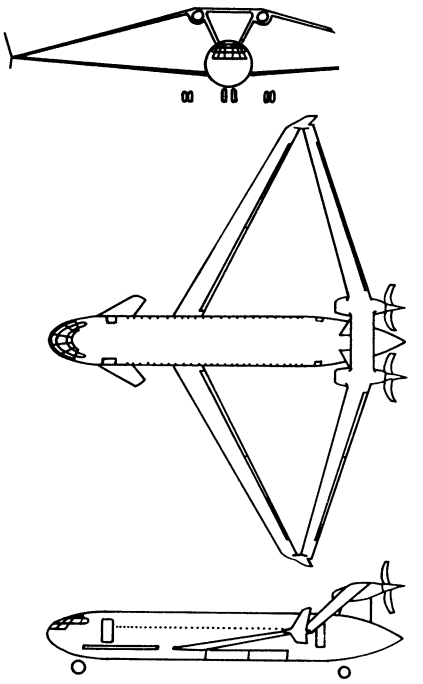

Fig. 14 Turboprop transport configuration with aft-mounted engines.

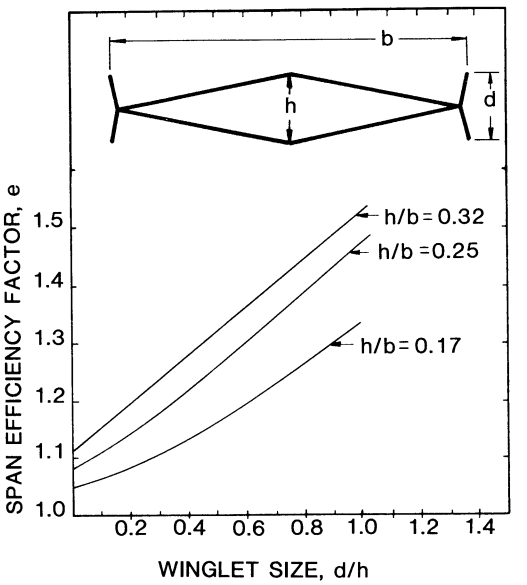

Fig. 15 Theoretical span-efficiency factor for joined wing with or without symmetric inclined winglets.

Reference 10 presents similar data on span-efficiency factor computed for inboard locations of the interwing joint. Moving the joint inboard causes a considerable loss of span efficiency; typically it falls to a level only 2 or 3% greater than the monoplane value.

Trim Drag

In general, it is not possible to obtain optimal span-loading at all lift coefficients while still maintaining trim.

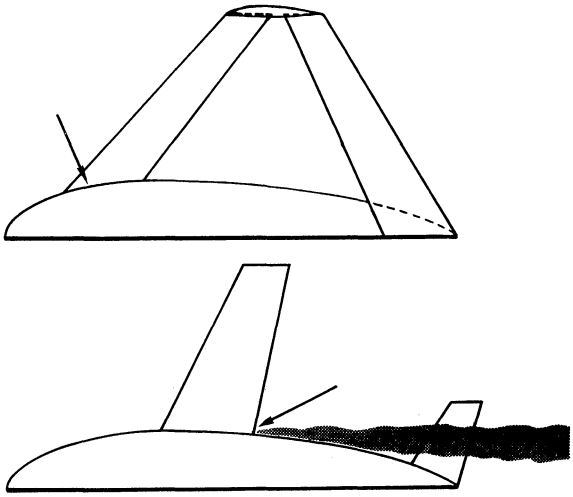

Fig. 16 Schematic comparison of wing-fuselage interference.

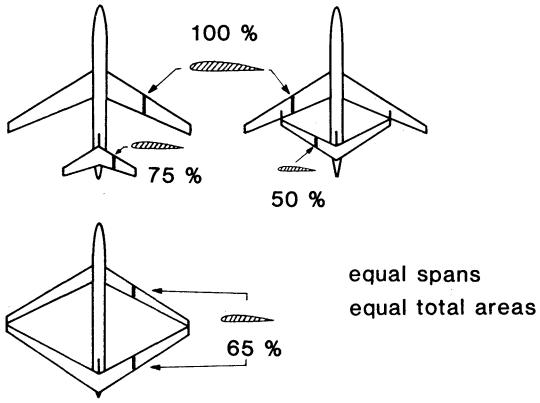

Fig. 17 Relative Reynolds numbers of mean geometric chords of front and rear lifting surfaces, for equal spans and equal gross projected areas.

The additional induced drag due to trim is generally slight for tip-jointed configurations because relatively small changes in loading of the center sections of the front and rear wings produce large moments. Furthermore, the winglets are typically located within a small longitudinal distance of the c.g.; hence, they can be optimally loaded without inducing unwanted pitching moments. Typically the trim drag in cruise is estimated at 1% of the induced drag calculated from the values of span-efficiency factor given above. For inboard-joint configurations, trim drag is comparable to that of conventional aircraft.

Experimental Corrections to Theoretical Induced Drag

In the tests described in Ref. 5, joined-wing and conventional-wing models were tested using the same fuselage. One of the principal objectives of this test was to examine the relative induced-drag characteristics of joined vs monoplane wings. Care was taken to compare the wings at equal chord Reynolds numbers and to subtract out fuselage drag measured at the appropriate angle of attack and Reynolds number. Wing spans and areas were matched, and the wing-joining member was made as small as possible to eliminate its endplate effect. Both wings were optimally twisted for the same design C_L of 0.645 (with the reference area S equal to the GPA).

The joined-wing model was similar to that shown in Fig. 2 but had a shorter nose and no canard. The joined-wing model had 10.8-deg (front) and −9.2-deg (rear) dihedral and, by the analytical method of Ref. 15, was predicted to

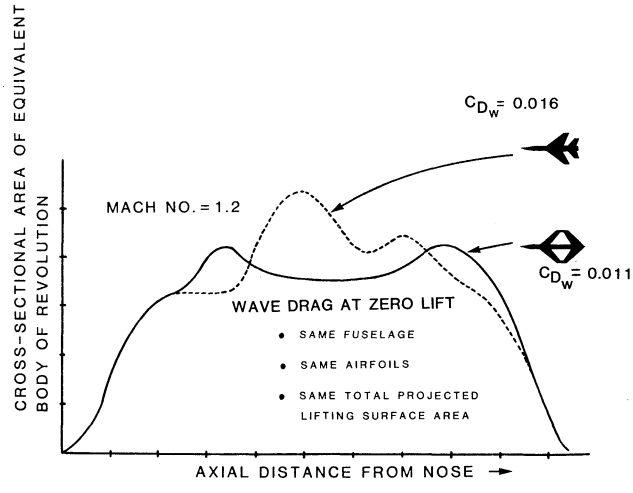

Fig. 18 Transonic wave drag comparison.

have a span-efficiency factor 1.0486 times that of the monoplane. The test results indicate that this ratio is actually 1.09. Thus, this particular joined wing achieves a span-efficiency factor 4% higher than the standard theory predicts. This occurs because the theory neglects the downward drift of the vortex sheet shed by the front wing.

Reference 17 describes similar comparative tests on monoplane vs nonjoined tandem wings, which showed a span-efficiency factor 14% higher than predicted by the theory. One would expect a higher gain for a tandem-wing system than for a joined-wing system since the tip regions on the former have a higher gap and stagger and are therefore more sensitive to vortex sheet drift.

Extensive free-vortex computations would be necessary to resolve the question of how much additional benefit to span-efficiency factor derives from the back-stagger of the joined wing. Pending such computations, it is tentatively recommended that the span-efficiency factors should be multiplied by the following ratio, which has been derived by considering the sweep angles of the quarter-chords of the wings of the model of Ref. 5 (+29 and −20 deg):

$$\frac{e_{\text{actual}}}{e_{\text{theoretical}}} = 1 + \frac{0.04(\tan\Lambda_F + \tan\Lambda_R)}{(\tan 29\ \text{deg} + \tan 20\ \text{deg})} \tag{3}$$

Offset Drag Polars

For an isolated lifting surface that is twisted and/or incorporates spanwise variations in camber, it has been shown[18] that the induced drag is described by an equation of the following form:

$$C_{D_i} = [(C_L - C_{LX})^2/\pi A e_x] + (C_{D_i})_{\min} \tag{4}$$

where C_{LX} and e_x are constants.

This form of drag polar is offset along both axes from the classical form of induced drag polar:

$$C_{D_i} = C_L^2/\pi A e \tag{5}$$

Note that the offset form arises even if the parasite drag is zero or invariant with C_L. Also, note that at a given lift coefficient the minimum achievable induced drag, corresponding to uniform downwash, is the same regardless of which form of polar is used. This minimum is obtained only at the design C_L if the polar is offset, but, for a wide range of off-design C_L, the drag increase over the nonoffset value is negligible.

The tests of Refs. 5 and 17 indicate that, for a given twist, the offsets along both axes are increased by combining airfoils in tandem or as joined wings. It is probable, therefore, that the offset effect is relatively large for joined and tandem

wings. Unfortunately, no theoretical analysis is available at present and no general guidelines can be given. An empirical correlation is given in Ref. 5 for the particular airfoils tested in that reference, but no basis for extrapolation to more general airfoils is yet known. A complicating factor is the fact that viscous effects add an additional offset, which is critically dependent on the extent to which leading-edge suction is developed.[19]

For joined wings that are optimally twisted to give minimum induced drag at a specified C_L, the induced drag at this "design" C_L may be computed from Eq. (5). For off-design conditions the following approach is tentatively suggested, based on Ref. 5 (p. 43): Increase C_{LX} by 0.15 above the two-dimensional viscous airfoil value; put e_x equal to $e-0.255$, and equate the induced drag computed by the offset polar to the nonoffset value at the design C_L.

Fuselage Interference

As with any airplane, the presence of the fuselage causes a loss in span-efficiency factor. This is generally less severe for a joined wing than a conventional wing because the rear wing is clear of the fuselage. Additionally, the rear wing may be able to reduce the nonuniformity of the downwash of the front wing so that the Trefftz-plane downwash distribution more nearly approaches its ideal uniform value. Empirically it is suggested that these factors should be taken into account by reducing the fuselage intereference penalty on e to one-half its value for a monoplane of the same ratio of fuselage diameter to wing span.

Wing Interference

None of the wind tunnel tests performed to date have shown any significant drag penalty due to adverse interference in the region of the wing joint. For example, the Rockwell model of Fig. 1, tested over the Mach number range of 0.4-0.95, displayed drag polars of normal appearance, with a minimum drag value only 7% greater than the computed drag of its isolated components.[4,21] For the model of Fig. 4, the measured minimum drag was 92% of the value computed by standard NASA drag prediction methods.[23] The major reasons for the absence of adverse interference are:

1) The airfoils do not overlap in plan view.

2) Each airfoil is designed to operate in the curved flowfield generated by lift on the adjacent airfoil (as will be discussed in the Section titled Airfoil Design).

Parasite Drag of Joined-Wing Aircraft

The following rules should be followed for low parasite drag:

1) Do not overlap the front and rear wings in plan view. This is likely to induce a venturi effect, which will increase drag. (None of the joined-wing wind tunnel tests performed to date have indicated any significant penalty due to interference at the joint, and it is believed that this has resulted from the absence of overlap.)

2) Locate the front wing root forward on the fuselage in a region of favorable pressure gradient. As shown in Fig. 16, this reduces the tendency to separation that occurs with conventional configurations where the wing root is located at the maximum width portion of the fuselage. (Although such separation can be reduced by fillets, these increase the wetted area of the configuration.)

3) Fillet the junction of the rear wing undersurface and the vertical tail to minimize separation. A T.E. "bullet" fairing of semicircular cross section should be used to anchor the fillet.

4) As shown in Fig. 17, for tip-jointed configurations, wing Reynolds numbers are lower than for comparable cantilever wings. Therefore, for tip-jointed configurations, consider the use of natural laminar flow airfoils. (Inboard-jointed configurations operate at Reynolds numbers similar to conventional wings; see Fig. 17).

Wave Drag

At low supersonic Mach numbers, joined wings have less zero-lift wave drag than conventional wings of similar L.E. sweep and total area. Figure 18 illustrates this for the Rockwell configuration of Fig. 1. Due to its smoother area progression, the joined wing has only 69% of the zero-lift wave drag of a conventional configuration of equal gross projected area and thickness/chord ratio.

Wave drag at finite lift is also low for joined-wing aircraft because the total lift is carried over a large fraction of the length of the vehicle. The self-bracing of the joined wing permits the use of very thin airfoils, giving further wave drag savings.

Airfoil Design

The lift on each airfoil of any joined-wing pair causes the other airfoil to be immersed in a curved flowfield (see Fig. 19). Because of this induced flow curvature, fair comparisons between joined wings and isolated wings cannot be made if the airfoils are constrained to be identical. This point has been demonstrated for biplanes by Addoms.[20] Thus, the design of airfoils for joined wings must consider the induced flow curvature, and design methods similar to those used for multielement airfoils should be employed, particularly for airfoils in the vicinity of the interwing joint.

For a full account of airfoil design for a transonic joined wing, see Ref. 21, which has been published in an abbreviated form as Ref. 4. For subsonic aircraft, some preliminary discussion of joined-wing airfoil design is given in Ref. 1, but much more remains to be done. The vortex-lattice program of Ref. 22, which yields optimum joined-wing twist and camber lines for specified pressure distributions, has proven to be useful in airfoil selection. This program typically leads to the camber/incidence relations shown in Fig. 20, for chordwise pressure distributions with a uniform pressure over the first 50% of the chord and a design C_L of 0.3. (Figure 20 is merely illustrative and may not be optimum or near-optimum for different configurations. For similar configurations, the camber and twist required for minimum trimmed induced drag at C_L other than 0.3 can be obtained by ratioing the camber and twist proportionately to C_L.) It is not essential to attain the optimum twist and camber exactly; linear or bilinear spanwise variations may be used instead. However, it is essential to "wash out" the front wing so that its tip has less incidence than its root, and the rearwing should be "washed in" with less incidence at its root than at its tip. The rear wing should also incorporate less camber than the front wing.

Simple model gliders of 12 to 24-in. span are of value in understanding the joined wing's structural and aerodynamic characteristics. Readers are encouraged to build such models, which should follow the above recommendations on twist and camber. The following approximate rules may also

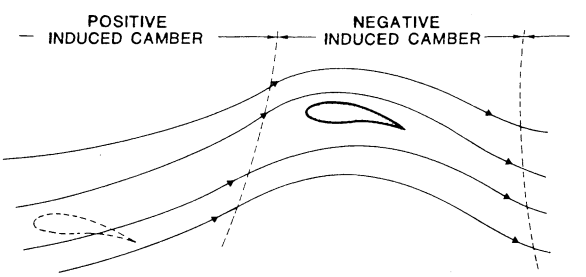

Fig. 19 Curvature of flowfield induced by rear wing on front wing, showing effective change of camber induced on front wing.

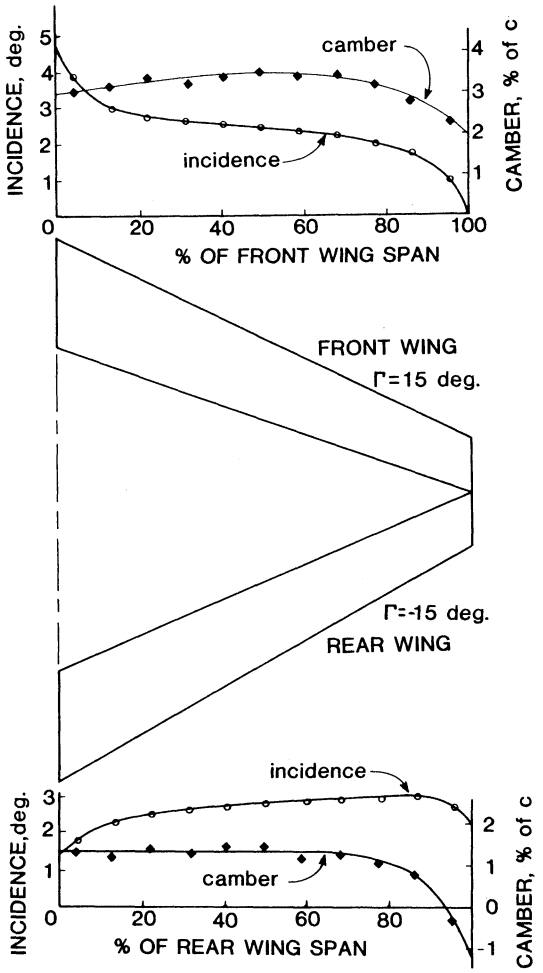

Fig. 20 Twist and camber for minimum induced drag at $C_L = 0.3$ (incompressible flow).

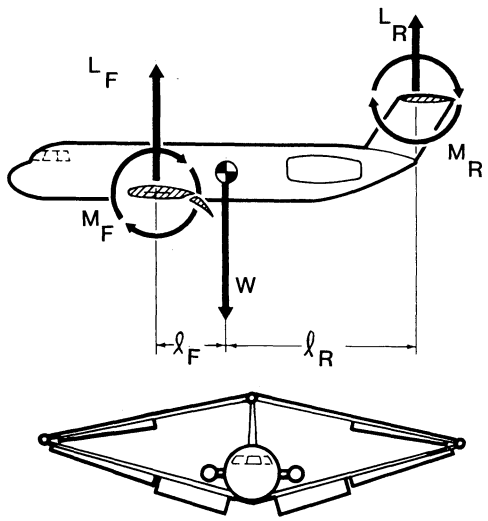

Fig. 21 Trimming for maximum lift coefficient.

be helpful. Typically the front wing root incidence should be 8 deg, decreasing linearly to zero at the tip, and the rear wing tip incidence should be zero to −1.0 deg at the tip, decreasing to −3.5 deg at the root. Relative to the type of curved plate airfoil that would normally be employed on the wing of a conventional model of this size, the front wing camber should be increased by 50% and the rear wing camber decreased by 50%. Both wings should be tapered, with approximately equal magnitudes of positive and negative dihedral.

For inboard-joint configurations there is an abrupt decrease in total (front-plus-rear) chord at the joint. A correspondingly abrupt increase in wing incidence just outboard of the joint is desirable, to maintain a smooth span-load distribution across the joint. Typically, a 1-deg jump in incidence of the front wing is required.

Further research is needed on joined-wing airfoil design. This should include consideration of very thin airfoils. For some applications these are desirable aerodynamically but not feasible with cantilever wing structures. Additional comments on airfoils are given at the end of the next subsection.

Planform and Airfoil Considerations for High Lift Coefficients

Certain guidelines must be followed to enable the joined wing to obtain high lift without excessive wing area. These guidelines include considerations of trim, as well as flow separation.

Trim Equations and Their Consequences for Airframe Geometry

Figure 21 shows the lift forces L_F and L_R acting at the aerodynamic centers of a joined-wing pair. When each wing (individually) is producing zero net lift, it produces a pitching couple M_O, as indicated. For 1-g steady flight, the lift and moment equations about the c.g. become (with notation as in Fig. 21)

$$L_F l_F + M_{OF} + M_{OR} = L_R l_R \tag{6}$$

$$L_F + L_R = W \tag{7}$$

It will be found for almost all statically stable joined-wing configurations that when the front wing attains its $C_{L\max}$, the rear wing lift required to maintain trim is less than the rear wing could generate, were trim not required. In other words, the front wing stalls first. This provides good stall recovery, but it is nevertheless undesirable for the front wing to stall while the rear wing is still far from stalling. If this occurs, it implies that the rear wing area is oversized from the viewpoint of generating the total maximum lift to meet the requirements of 1g and maneuvering flight. One would prefer the front wing to stall when the rear wing is almost at its $C_{L\max}$. To achieve this, certain principles must be followed in designing the overall airframe geometry, especially the planform. These principles can be derived by manipulating Eqs. (6) and (7) as follows. From Eq. (6),

$$L_R = L_F(l_F/l_R) + (M_{OF} + M_{OR})/l_R \tag{8}$$

whence

$$\frac{C_{L_R}}{C_{L_F}} = \frac{S_F}{S_R} \cdot \frac{l_F}{l_R} + \frac{(M_{OF} + M_{OR})}{C_{L_F} S_R l_R} \tag{9}$$

The quantity $(S_F l_F)/(S_R l_R)$ in Eq. (9) is always less than unity for a statically stable aircraft. Even for identical front and rear wing areas and equal (positive and negative) sweep angles, $l_F/l_R < 1$ because the overall vehicle aerodynamic center (a.c.) is nearer to the a.c. of the (isolated) front wing than the a.c. of the (isolated) rear wing. This is because the C_{L_α} of the rear wing is $(1 - d\epsilon/d\alpha)$ times its own isolated C_{L_α}. The following principles should be followed to obtain the highest possible value of the first term in Eq. (9).

1) Decrease the ratio of front wing lift-curve slope to rear wing lift-curve slope by employing less sweep on the rear wing.

2) Increase the ratio of rear wing/front wing chord to move the a.c. aft.

3) Reduce the effective $d\epsilon/d\alpha$ at the rear wing by using a large centerline gap (i.e., make the fin tall). It is also

beneficial to employ winglets since these reduce the average $d\epsilon/d\alpha$ at the rear wing.

4) Take advantage of the large pitch damping of the joined-wing configuration to move the c.g. aft without sacrificing maneuver margin. (Generally maneuver margin, not static margin, is the key stability parameter.) If control configured vehicle (CCV) technology is allowable, it should certainly be employed so that the maneuver margin can be made negative. This increases trimmed $C_{L\max}$.

Turning now to the second term in Eq. (9), the key consideration is to make the M_O terms large and positive. This leads to the following guidelines:

1) Do not employ equal flap deflections across the span of each wing. Instead, employ maximum flap deflections on the inboard front wing and outboard rear wing, as shown in the upper half of Fig. 21, to make each wing's M_O as nose-up as possible.

2) Leading-edge devices near the root of the front wing are beneficial.

3) A low-aspect ratio canard can provide appreciable nose-up moment with little forward a.c. shift.

4) Where practicable, the fuselage should be shaped (i.e., cambered) and the wing incidence selected to provide positive C_{mO}.

The foregoing recommendations have emphasized overall airframe geometry rather than local aerodynamic design (e.g., of airfoils and flaps). It is, however, particularly important that the front wing root airfoil be selected to give a high local $C_{L\max}$, as discussed below.

Airfoil Considerations for High Lift

Figure 22 (redrawn from Ref. 24, Sec. 16, p. 4) shows that a swept-back wing obtains a high $C_{L\max}$ near its root. This effect is doubly beneficial for the joined wing since, besides increasing $C_{L\max}$ directly on the front wing, it also provides a nose-up moment that allows the rear wing to be trimmed at a higher C_L.

As described later, wind tunnel tests on joined wings (Refs. 4-6, 21) show no indications of the pitch-up associated with swept wings, possibly because the joined wing tips are only a short distance aft of reasonable c.g. locations. There may also be a beneficial slat effect of the rear wing, which delays stalling of the front wing tips. Design of joined-wing airfoils for high lift should include considerations of the induced angle of attack and the flow curvature induced by each wing on the other. This may require the use of multielement or biplane airfoil design techniques.

Effect of Canard on Maximum Lift

The configuration of Fig. 2 was tested with and without the 60% sweep canard, and also with a conventional wing and tail. The canard exposed area was 11.7% of the GPA of the front plus rear joined wings. Strakes were also tested (see Fig. 23). These had an exposed area of 2.3% of the GPA. Comparisons of $C_{L\max}$ were made at equal Reynolds numbers for each configuration. It was found that the L.E. vortex shed by the canard induced considerable augmentation of the lift of the front wing. A full description of the comparison is given in Ref. 5. The essential points are summarized below.

For fair comparison of lifting capabilities of alternative wing systems, the reference areas employed to define lift coefficient must be equitable. Reference 5, therefore, compares measured trimmed C_L of joined vs conventional wings by referring each C_L to the total exposed area of the appropriate lifting surfaces, including the canard and strake when present. This lift coefficient will be denoted as C_{LE}. At equal dimensional static margins and equal Reynolds numbers, with essentially identical airfoils, the relative trimmed C_{LE} values determined from wind tunnel tests compared as follows: conventional, 100%; joined wing, 104-107%; joined wing plus canard, >119%.

The > sign indicates that, as shown in Fig. 23, the C_L-alpha graph was still rising at the highest angle of attack tested (22 deg).

As noted in Ref. 10, the wind tunnel data of Ref. 5 show that the above ratios are maintained over a wide range of stable static margins. At forward c.g.s the vortex lift generated at the front wing root and on the canard provides the required nose-up trimming moment. If this effect can be maintained at full scale, the joined wing should be able to trim over a wide c.g. range without significant loss of maximum lift.

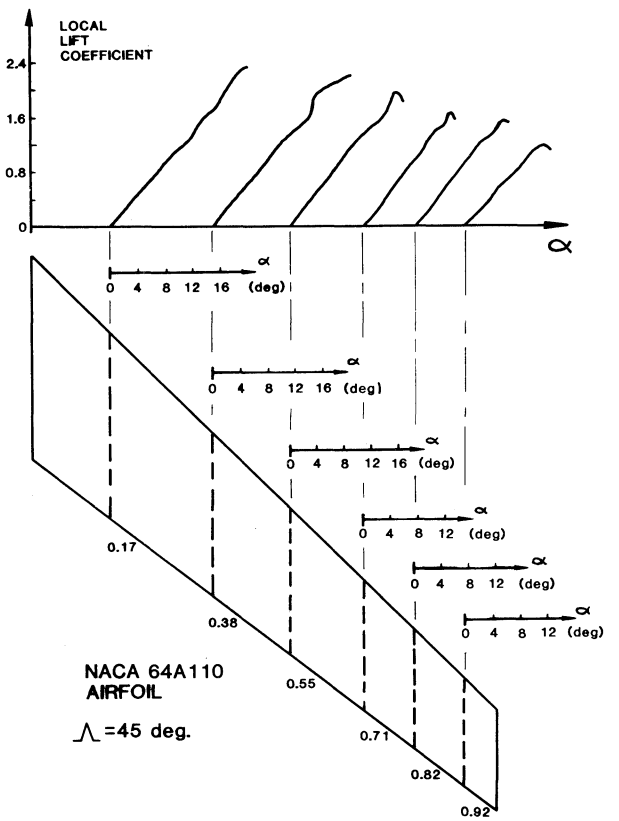

Fig. 22 Measured sectional lift vs angle of attack of a swept wing with no flaps.

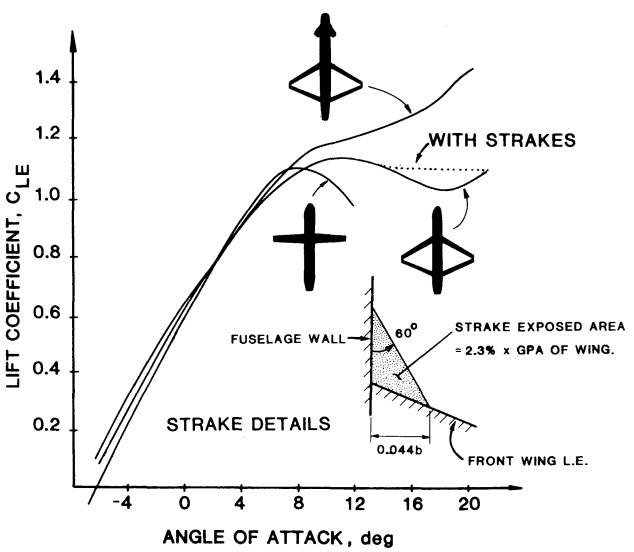

Fig. 23 Measured variation with angle of attack of untrimmed lift coefficients referred to total exposed areas of all lifting surfaces.

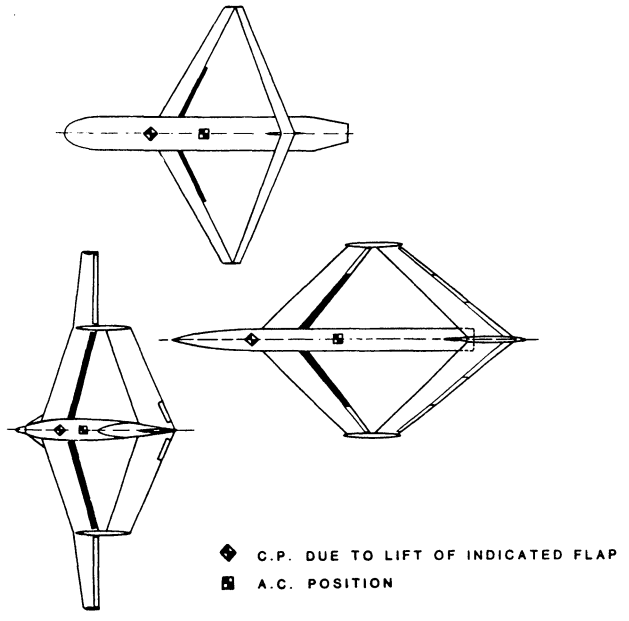

Fig. 24 Aerodynamic center and flap c.p. locations from low-speed wind tunnel tests.

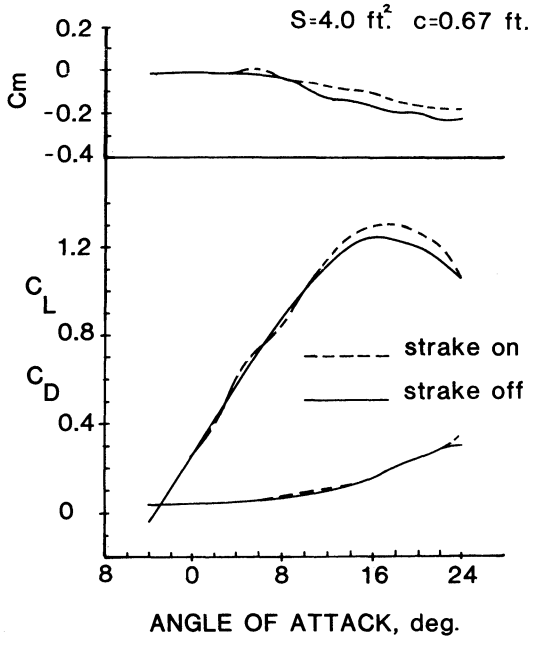

Fig. 25 Effect of strakes on longitudinal characteristics of agricultural airplane model.

IV. Stability and Control

Longitudinal Stability

Because of the large number of combinations of geometric parameters possible for a joined-wing pair, it is not feasible to give handbook-type formulas for aerodynamic center location. However, Ref. 10 presents a series of DATCOM style charts showing a.c. location as a function of front/rear sweep, dihedral, taper, and other geometric parameters, as well as Mach number. These charts were computed by vortex-lattice methods, which have demonstrated good agreement with measured a.c. locations, such as the typical a.c. locations shown in Fig. 24.

As discussed below, for some configurations this procedure predicts an a.c. location that is accurate at low angles of attack but is slightly too far forward at high angles of attack below the stall.

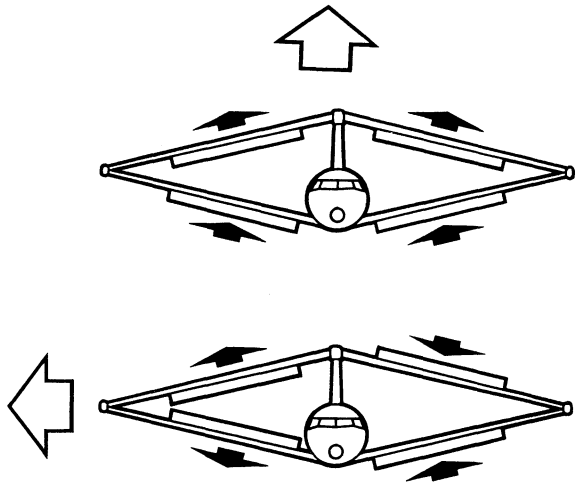

Fig. 26 Direct lift and sideforce capabilities.

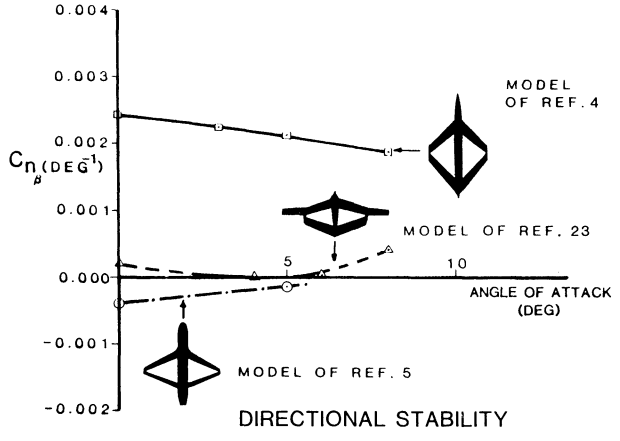

Fig. 27 Yawing moment due to sideslip from low-speed wind tunnel tests.

Nonlinear Pitching Moment

Some, but not all, of the wind tunnel tests that have been performed on joined-wing configurations have shown a mildly nonlinear pitch-down characteristic at moderate and high angles of attack below the stall. At these conditions the a.c. tends to move aft of its low-angle-of-attack position. This phenomenon is clearly shown in Fig. 25, from Ref. 23, which shows low-speed test results for the configuration of Fig. 4 with and without strakes. These strakes, shown in Fig. 24, employ 55-deg leading-edge sweep of the wing GPA. At angles of attack above 8 deg, with strakes off, the a.c. shifts aft by 13% of the distance between the front and rear wing quarter-chords. With strakes on, this shift is only 6%. Similar trends occurred in tests of a tandem-wing nonjoined configuration.[17] The joined-wing model of Fig. 2 also exhibited this tendency with the canard off,[5] but the model of Fig. 3 (unpublished data) showed an extremely linear pitching moment variation with lift up to the stall. The model of Fig. 1, tested over a Mach range of 0.4-0.95, showed only a very slight pitch-down effect at all Mach numbers.[4, 21]

Reference 23 ascribes the pitch-down to partial stalling of the front wing. This causes the lift-curve slope of the front wing to reduce, and it also reduces the downwash on the rear wing, so its lift increases. The net result is that the overall configuration lift-curve slope remains approximately constant, but the pitching moment slope becomes more negative, because of the large moment arms of the front and rear wings about the moment center. Since such partial stalling (or partial loss of leading-edge suction) is highly dependent on Reynolds number and on model configuration details and

surface condition, it is hard to predict. However, one would expect it to decrease as Reynolds number is increased, so it should be less apparent at full scale.

Strakes

The model of Fig. 4 was tested with and without small strakes. The strakes reduced the pitch-down tendency, although they did not eliminate it. This is illustrated in Fig. 25. Small strakes with wetted area equal to 2.5% of the joined-wing wetted area were also tested on the model of Fig. 2 (canard off). They increased $C_{L\max}$ slightly but did not affect the pitching moments. The model of Fig. 2 employed a 9%-thick airfoil, whereas that of the Fig. 4 model was 19% thick. The strakes would be expected to produce larger changes when fitted to the thicker wing since it does not generate as much vortex lift as the thinner wing. The strake-induced vortex lift provides a pitching moment that opposes the pitch-down caused by partial loss of leading-edge suction on the front wing.

Canard

Adding the 60-deg sweep canard to the configuration of Fig. 2 caused the pitch-down tendency to be replaced by a pitch-up due to the vortex-lift generated on the canard and the effect of the canard vortices in delaying the stall of the front wing. It appears that rear wing elevators (not tested) would have been adequate to control the pitch-up and would have increased the total lift still further. For the model as tested, trim was obtained by canard incidence.

Longitudinal Control

Pitch Attitude Control

Elevators may be mounted on either or both the front and rear wings and also on the canard, if one is employed. The center of pressure of the additional lift generated by front wing elevators is generally located some distance forward of the elevators, as illustrated on Fig. 24. This figure shows the c.p. locations for three configurations as determined from wind tunnel tests. (These c.p. locations are close to the locations predicted by vortex-lattice methods.) The c.p. locations are further forward than the elevator because of the downwash induced on the rear wing. This reduces the total lift generated by downward elevator deflection but increases the nose-up pitching moment. This moves the c.p. forward because the distance of the c.p. ahead of the moment center is equal to the incremental pitching moment divided by the incremental lift.

In general, rear wing elevators produce negligible effects on the lift of the front wing, and their c.p. location can be predicted by standard methods, considering the rear wing in isolation. The large number of parameters involved precludes simple formulas for the c.p. location and effectiveness of front wing elevators, but Fig. 24 provides some guidance.

Direct Lift Control

As indicated from Fig. 26, if front wing and rear wing elevators are deflected downward by equal angles measured about the appropriate hinge lines, the resultant lift acts close to the moment center. Thus, by combining front and rear wing elevators, direct lift control is obtained. In general, the elevator deflections required for direct lift control will not be equal on both wings. For the wind tunnel model of Fig. 1, equal elevator deflections provided direct lift because the configuration employed equal sweep angles on front and rear wing leading edges. This gave a large sweep angle to the hinge line of the rear wing elevator (54 deg vs 26 deg for the front elevator). As a result, the pitching moment effectiveness of the rear elevator was reduced to a level comparable to that of the front elevator in the presence of the rear wing.

The optimum form of pitch control is not known, but one would expect that some combination of front elevator and direct lift control would be desirable to facilitate takeoff rotation and liftoff. Such a control arrangement would also improve flying qualities by reducing the lag between the application of pitch control and the buildup of normal acceleration in the desired direction.

Lateral—Directional Stability

The variation of yawing moment with sideslip for the model of Fig. 1 was found to be very linear. As shown in Fig. 27, the model attained a normal level of directional stability ($C_{n\beta} = 0.0025$ per deg). The earlier models of Fig. 2 (canard off) and Fig. 4 did not have satisfactory directional stability. This was unexpected, since both of these models were expected to derive a substantial directional stability contribution from the anhedraled rear wing, which presents considerable side area. However, Ref. 10 has recently explained the phenomenon. Reference 10 analyzes this effect and shows how the low $C_{n\beta}$ stems from the "vane" effect of the vertical tail on the rear wing. The anhedral of the rear wing augments $C_{n\beta}$, but the vertical tail decreases the local sideslip angle at the rear wing to approximately 50% of the overall sideslip angle of the aircraft. The effect was counteracted in the tests of Ref. 23 on the model of Ref. 4 by adding a vertical tail extension above the rear wing. The net conclusion is that, because of the above-mentioned vane effect, the anhedraled rear wing is only about 50% effective in providing directional stability. If directional stability proves to be low, either fin area and/or rear wing anhedral should be increased. As indicated by the Fig. 1 configuration, the fin area required for directional stability is not excessively large.

The rolling moment due to sideslip can be set to normal levels by tailoring the front and rear wing dihedral angles. Since the rear wing is immersed in the sidewash of the front wing, it is less effective in generating rolling moments. Hence, with equal and opposite dihedral and sweep angles, the front wing dominates, and the net $C_{l\beta}$ is markedly negative. References 4, 5, 10, 21, and 23 provide data on joined-wing rolling moments due to sideslip.

Roll Control

Figure 28, from Ref. 5, shows wind tunnel data on the ratio of yawing moment to rolling moment induced by ailerons mounted on the rear wing of the model of Fig. 2 (canard off). No aileron differential was employed; nevertheless, the ailerons generate only a small yawing moment. This desirable result occurs because (as shown by the inset diagram on Fig. 28) the aileron sideforces produce a yawing moment that opposes the yawing moment due to differential aileron drag. Conversely, it was found in Ref. 5 that front wing ailerons produced severe adverse yaw. Front wing ailerons appear to be less desirable than rear wing ailerons and may require considerable differential if the front wing has a large dihedral angle.

The selection of aileron geometry for joined wings must take into account the above factors and must also allow for the high rigidity of joined wings, which improves aileron effectiveness.

For aircraft requiring a high roll rate it may be desired to fit ailerons on both the front and rear wings. This is permissible if the front wing has little dihedral. The greatest roll control power is obtained by mounting the front wing ailerons slightly inboard so that their upwash/downwash increases the rolling moment on the outboard sections of the rear wing. This is discussed in Refs. 10 and 25.

Yaw Control

Rudder effectiveness was examined in Ref. 23 for the agricultural airplane configuration of Fig. 4 and was found

to be low. Contributing factors were the 18%-thick airfoil of the vertical tail and the low Reynolds number of the test (approximately 50,000 based on mean chord of the rudder). Reference 23 suggests that the rudder effectiveness may be low because of its enclosure within the channel formed by the front and rear wings. However, flight tests on several radio-controlled joined-wing models have shown adequate rudder effectiveness, so this question remains open.

Direct Sideforce Control

Direct sideforce capability is inherent in the joined wing and requires no vertical surfaces, as shown in Fig. 26. The transonic wind tunnel tests described in Refs. 10 and 21 have verified this capability but have not explored it in detail or optimized the ratio of front to rear wing control surface deflections to minimize rolling and yawing moments.

V. Design Integration

The Importance of Design Integration

Having described the aerodynamic and structural principles of joined wings, their use in complete airframes will now be discussed. Although it is possible to take an existing fuselage for a conventional wing-plus-tail and mate it to a joined wing, this rarely produces the best results. It is better to design a completely new airframe. The preliminary design of this new airframe involves some novel considerations with regard to fuel tankage, landing gear, wing/fuselage geometry, and the use of a canard in addition to the joined wing. These and other aspects of design, such as crashworthiness and wing folding, are discussed below.

Fuel Volume

Figure 29 compares the wing fuel tank volume available from conventional and joined wings of the same span, GPA, and thickness/chord ratio. To match the fuel capacity of the conventional wing, a tip-joined joined wing must employ the extended box spar that is also needed for minimum structural weight (see Fig. 6). The comparative fuel volumes shown in Fig. 29 assume that the fuel occupies the space between the wing shear webs, i.e., 5-75% of the joined-wing chord, vs 15-65% of the cantilever-wing chord. This reduces the chord available for flaps on the joined wing. The tip-jointed configuration should also carry fuel in both the front and rear wings. This is not necessary for an inboard-jointed configuration which, as indicated in Fig. 29, can accommodate more fuel than a conventional wing due to its use of an extended box spar in the joined portion of the wings, with a normal box spar in the cantilever portion.

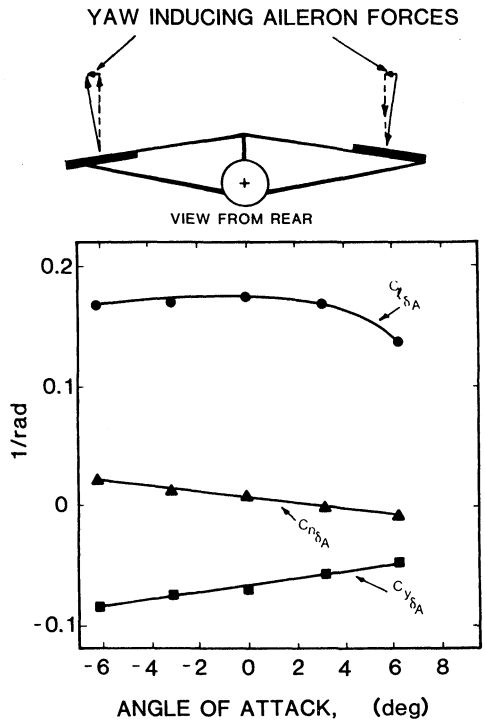

Fig. 28 Measured aileron roll, yaw, and sideforce with zero aileron deflection and rear wing ailerons only.

Landing Gear

Reference 10 describes several alternative landing gear concepts for joined-wing transports. Figure 30 illustrates one concept; this can employ three main wheels, a single main wheel with outriggers, or dual main wheels that retract into the interwing fairing. Whatever landing gear arrangement is selected, the main wheel location and ground angle should be tailored to permit easy nosewheel raising. A positive ground angle may be necessary.

Propulsion System Integration

The joined-wing structure is well suited to pusher or tractor engines located in the "armpit" formed by the rear wing and twin fins as shown in Fig. 14. This engine location has several advantages. It provides a rigid engine mounting and moves the propellers aft of the passenger cabin, thus minimizing cabin noise. It permits short landing gear and allows the engines to be lowered to the ground for servicing, although the local wing and fin structure must be protected from engine components in the event of disintegration. The principal disadvantage is the high thrust line, which causes power-induced trim changes. The prospects of countering these trim effects by local twisting of the wing and/or downthrust deserve investigation. If this location is not acceptable, wing- or fuselage-mounted engines may be employed.

Wing Folding

Figure 31 illustrates a wing folding system employing front and rear wing hinges on a common axis. Reference 1 describes other systems of folding for missile applications, where the folded wing must be accommodated within the missile fuselage.

Crashworthiness

The joined-wing airplane offers a potential advantage in this regard. Placing the front wing root toward the nose of the fuselage enables the joined wings to brace the passenger compartment so that it is less likely to buckle in a crash. The front wing becomes the major energy-absorbing structural element.

Ditching characteristics of joined-wing aircraft are expected to be satisfactory since the airplane floats supported by the front wing, winglets and tip tanks.

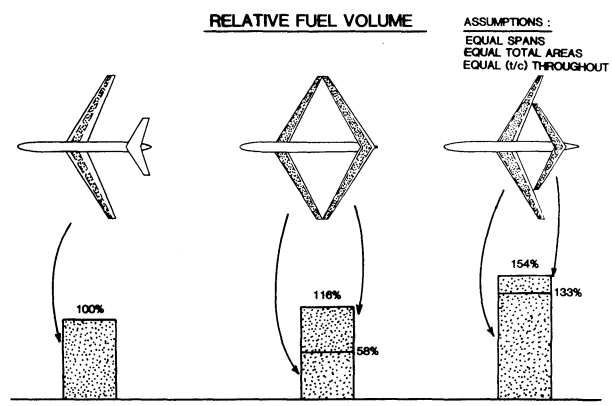

Fig. 29 Fuel volume comparison.

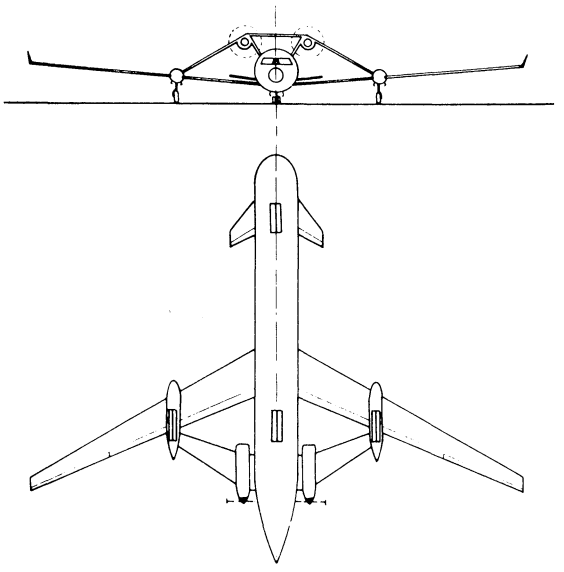

Fig. 30 Configuration employing landing gear with three main wheels.

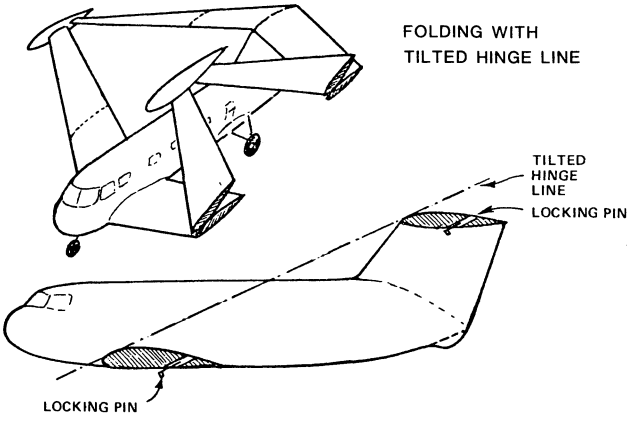

Fig. 31 Wing folding system employing front and rear wing hinges with a common axis.

Wing/Fuselage Geometry

As described in Secs. I and II, the structural weight savings of the joined wing are greatest for wings having 1) moderate sweep and 2) large dihedral angles (positive and negative). This combination is most compatible with a fuselage having relatively low fineness ratio and a tall vertical tail. For many applications, fuselages of low fineness ratio are desirable from the viewpoint of passenger comfort, landing gear accomodation, and minimum weight. If a long, slender fuselage must be employed, it may be best to combine it with a joined wing plus a canard. This combination provides adequate pitch trim capabilities while avoiding too low a ratio of sweep to dihedral for the joined wing. Figure 14 illustrates such a configuration, incorporating a highly swept canard that is retracted in cruise. The canard serves as a high lift system, allowing the wing leading edges to remain free of high lift devices, thus facilitating laminar flow.

VI. Joined Wing Applications

Example Designs

The joined wing has a wide spectrum of applications, ranging from hang gliders to space shuttles. Some selected designs are briefly discussed below.

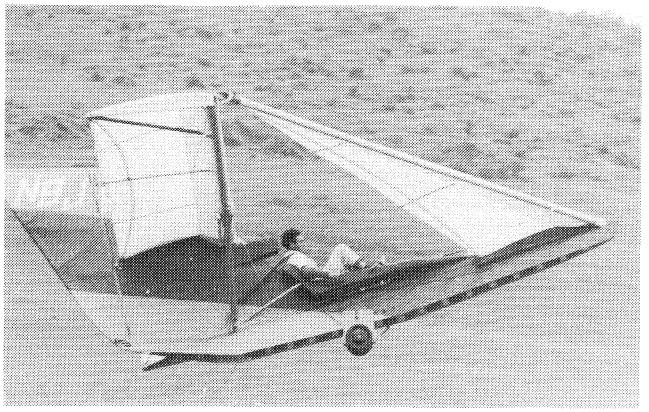

Fig. 32 The author's 1974 primary glider.

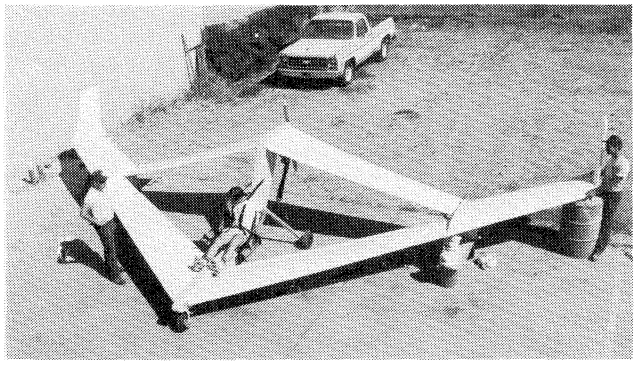

Fig. 33 Summit Aircraft Corp. Trident ultralight airplane.

Figure 32 shows a primary glider (the Skyrider), designed, built, and flown in the early 1970s by the writer, assisted by Mr. Dana Lake and others.[2, 26] The original goal of joining the wings on this glider was to obtain crash resistance and pilot protection. It became apparent that the joined-wing principle also offered other, more general advantages, as described earlier in this paper. Therefore, the Skyrider glider was not developed further, and the main effort of joined-wing research shifted to fairly general structural analyses and exploration of joined-wing aerodynamics via theory and wind-tunnel models. Following the validation of the basic concept by such research, the effort is currently turning toward design studies, construction, and flight testing of prototype manned aircraft.

Figure 33 shows an ultralight airplane (the Trident T3), produced by Summit Aircraft Corp., Denton, Texas.[27-29] This aircraft is largely of composite construction and incorporates extremely thin, highly cambered airfoils, made possible by the self-bracing joined wing. Pilot protection and good flying qualities were prime design goals for this aircraft, which was designed by Mr. David Lund of ACA Industries, Inc., and first flew in January 1985.

Figure 34 illustrates a concept for a high-altitude RPV designed for long endurance flight at altitudes above 60,000 ft. Structure weight is of extreme importance for such aircraft, yet the drag of bracing wires and struts is undesirable. The joined wing meets the weight requirement while providing the robustness required for rough landings in addition to climbs and descents through turbulence.

Figure 35 presents an artist's concept of another application. This figure illustrates the application of a joined wing to an executive jet. Applications to cruise missiles, ASW patrol-type naval aircraft, and agricultural aircraft have been shown in Figs. 2, 3, and 4, respectively, and various transport concepts (e.g., Fig. 14) are discussed in Ref. 10.

The joined wing has outstanding potential for V/STOL aircraft because it offers light structure weight and a conve-

nient location for the lift engines near the c.g. yet distant from the lifting surfaces, so that suck-down and interference are minimized. This is illustrated in Fig. 36.

Figure 37 shows a radio-controlled model of a manned research airplane (the JW-1), intended to gain experience of joined-wing flying qualities. This aircraft employs the fuselage and engines of the existing NASA AD-1 oblique-wing research airplane to provide a low-cost research and demonstrator vehicle. Reference 25 provides a full discussion of this aircraft.

To conclude this brief sampling of joined-wing applications, Fig. 38 shows a space shuttle orbiter concept. Reductions in both structure weight and induced drag were prime design goals. Leading-edge heating is estimated to be similar to existing orbiter configurations.

The above list of concepts and designs provides only a small selection of the possible applications of the joined wing.

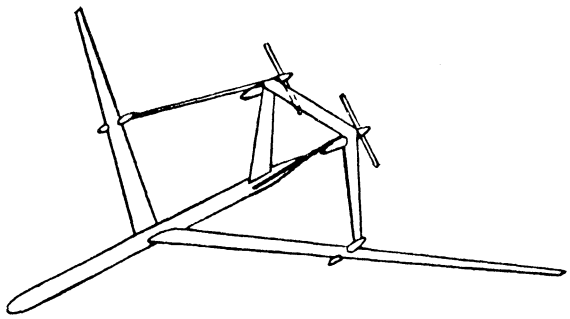

Fig. 34 High-altitude remotely piloted vehicle.

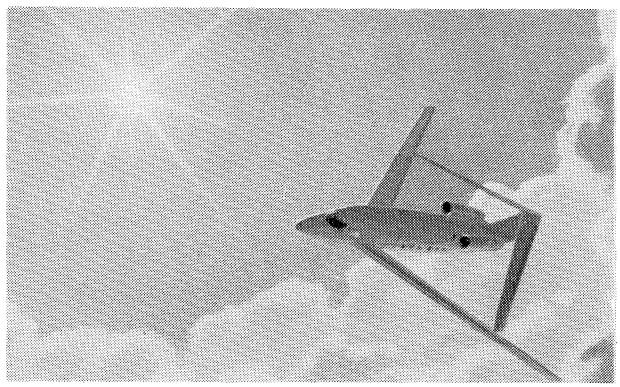

Fig. 35 Concept for an executive jet airplane.

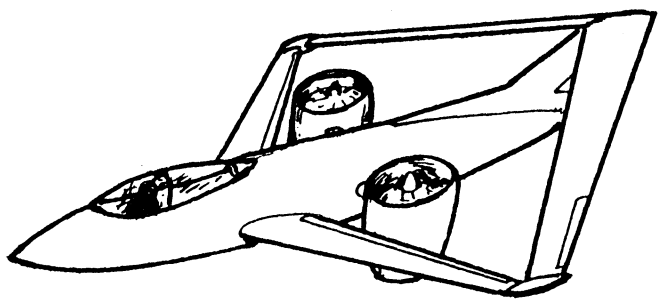

Fig. 36 Schematic Drawing of joined-wing V/STOL aircraft.

Performance Benefits of the Jointed Wing

The benefits provided by the joined wing depend on its application and the design goals. For some applications, weight saving may be of prime importance; for others, low wave drag and suitability for thin airfoils may be decisive. Since the joined wing can provide both aerodynamic and structural advantages, a full assessment requires the use of an aircraft design synthesis program to size an optimal design. For rapid assessments of the impact of the joined wing on performance, a number of shortcut methods may be used. For example, one may assume that no aerodynamic advantage is taken from the joined wing and that it is employed only to save structure weight. The weight saved may be traded for an equal weight of payload or fuel. Leaving the aerodynamic characteristics unchanged, the effect on range can then be assessed by the Breguet formula. To illustrate this approach, we consider a 155-passenger propfan transport design from Ref. 30.

Reference 30 describes a twin-engine transport having a gross weight of 140,000 lb, which consumes 19,552 lb of fuel to fly its maximum range of 1479 n. mi. The wing weight plus horizontal tail weight total 17,431 lb. From Figs. 7 and 8, 40% of this weight (i.e., 6972 lb) could be saved through replacing the wing and tail by an aerodynamically equivalent joined wing. If this weight is replaced by an equal weight of fuel, the relative range is given by the Breguet formula as

$$\frac{\text{Range of joined wing airplane}}{\text{Range of conventional airplane}} = \frac{\ln\left\{1+\dfrac{19{,}522+6{,}972}{120{,}478-6{,}972}\right\}}{\ln\left\{1+\dfrac{19{,}522}{120{,}448}\right\}} = 1.396$$

Thus, in this application, the joined wing gives an increase in range of 39.6%.

If desired, the joined wing could be used to increase span at the same weight, thus reducing induced drag. It could also be employed to permit thinner airfoils, giving faster cruise speeds. For unchanged range the joined wing could be used to increase the number of passengers. Allowing 300 lb per passenger to include fuselage structure, seats, and baggage, and an allowance for fuel used to overcome the drag of the enlarged fuselage, the number of passengers would increase by 23, from 155 to 178. With a break-even load of 110 passengers, this would change the potential airline profit on direct operations by a factor of $(178-110)/(155-110)=1.51$, i.e., an increase of 51% in potential profit. (Even allowing as much as 400 lb per passenger for fuselage structure, etc., the number of passengers would increase by 17 and the potential profit by 38%.

The joined-wing is at an early stage in its development and much data are still unpublished. In addition, the space available for this paper has not permitted discussion of many of the subtleties and refinements of joined-wing design. Therefore, the reader who wishes to evaluate the potential benefits of the joined wing for any specific application should contact the writer to obtain the most up-to-date information.

New Technology and the Joined Wing

Recent advances in aircraft design have developed new technology, e.g., composite materials, laminar flow airfoils, and control configured vehicles having relaxed static stability. The joined wing does not depend upon any of these new developments although it can make good use of all of them. For example, laminar flow is more easily obtained at the lower Reynolds numbers characteristic of tip-jointed joined wings. Composite materials are well suited to the non-uniform chordwise distribution of structural material that is optimum for joined wings (Fig. 6). Relaxed static stability

permits higher rear wing loadings, decreasing the total wing area required to lift the aircraft at takeoff and landing. The above examples show that the joined wing is synergistic with new technology.

The results obtained to date on the joined wing have not assumed any new technology. This restriction has been imposed so that comparisons between joined-wing and existing conventional aircraft could be made on a fair basis. In practical aircraft design, full advantage should be taken of new technology, and this is particularly true for the joined wing, because of its synergy with the technology advances cited above.

VII. Conclusions

1) The joined wing provides advantages over a conventional wing-plus-tail arrangement, including: a) lighter weight and higher stiffness, b) less induced drag, c) reduced transonic and supersonic drag, and d) built-in direct lift and sideforce capability.

2) Experimental data show that the joined wing has good stability and control in normal flight and at the stall.

3) The joined wing can provide reductions in parasite drag through smaller lifting surface areas, reduced wing-fuselage interference, and suitability for thin airfoils. These beneficial effects offset the effects of lower wing Reynolds numbers such that overall savings in parasite drag can be achieved.

4) Although the joined wing is synergistic with new developments such as composite materials, laminar flow airfoils, and control configured vehicles, it does not depend on new technology. Hence, it can provide the above advantages with short development times and low risk.

5) The joined wing is a highly integrated concept involving structures and aerodynamics. Coordinated efforts in both these technical areas are required to maximize the advantages of the joined wing.

Appendix: Related Configurations

Aircraft configurations having connected tandem wings have been proposed since the earliest days of aviation, (e.g., the Henson and Warren-Young projects of Refs. 31 and 32). Most of these proposals did not progress to the stage of flying manned aircraft, and none of them included the special geometric and structural features of the type of joined wing that is the principal subject of this paper. Therefore, they will be referred to as connected-wing rather than joined-wing configurations. A full historical summary would far exceed the space limitations of the present paper, so details will be given of only the two connected-wing airplanes known to have flown successfully. These are the 1922 Platz glider and the 1932 Brown airplane.

The Platz Glider

Figure 39 shows the Platz glider. This has been described in various references. The primary source of information is Ref. 33, but Ref. 34 is more accessible. The glider was designed by Fokker's chief designer, Reinhold Platz, and appeared in two versions during the early 1920s. Platz also constructed a modern version in 1963. The glider employed a structure in the form of a cross, consisting of a transverse spar, which formed the leading edge of the rear wing, attached to a longitudinal spar, which served as a fuselage. To these spars Platz attached for-and-aft sails, forming tandem wings. The root of each foresail was attached to a pivoted root rib, the trailing edge of which was held by the pilot. By moving these trailing edges in unison, the pilot obtained pitch control; roll control was obtained by differential movements. No fin or rudder was fitted. Approximate dimensions of the glider are: span, 24.6 ft; length, 16.2 ft.

The Platz glider flew well but did not influence glider design and passed into obscurity. One reason for this may have been that the unbraced spar arrangement was relatively heavy compared to the strut-braced gliders of its era. The gap between the front left and right wings also would have caused considerable induced drag. Regardless of these deficiencies, the Platz design deserves admiration for its originality and remarkable simplicity.

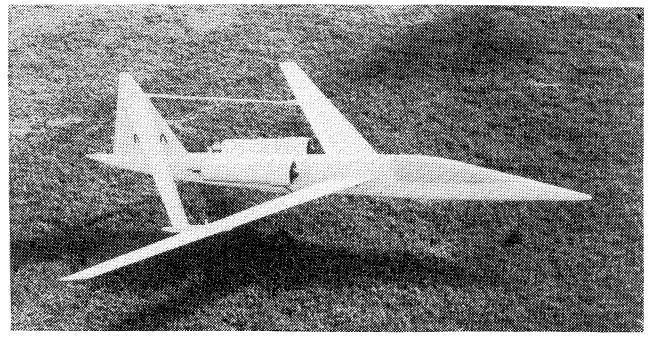

Fig. 37 Radio-controlled model of JW-1 research airplane design.

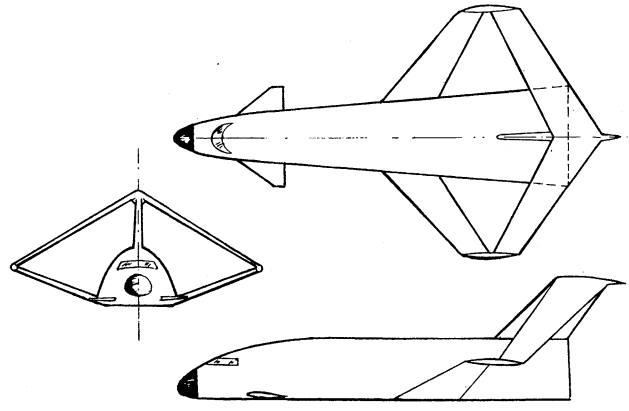

Fig. 38 Joined-wing space shuttle orbiter concept.

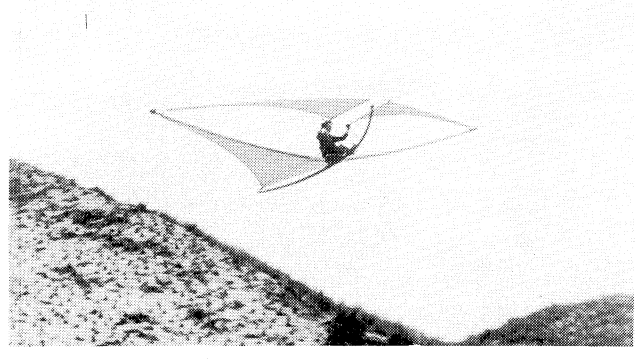

Fig. 39 1922 Platz glider.

The Brown Airplane

This unnamed aircraft was designed by Ben Brown of the University of Kansas around 1932. It is shown in Fig. 40.[34] It employed swept-back and swept-forward wings arranged to form a diamond shape in plan view but (unlike the joined wing) not in front view. A third wing, equal in chord to each of the others, acted as a strut. The Brown airplane made cross-country flights and performed loops. The only flying qualities deficiency of which the writer is aware is that the rudder was relatively ineffective for taxiing, due to its location ahead of the slipstream of the pusher propeller. The drive shaft system included a dry clutch to absorb torsional vibration and performed well. The Brown airplane faded away without influencing other airplane designs. The design can be criticized because of the low Reynolds number of each of the three equal-chord wings, but the major reasons

for its lack of impact on the trend of aviation history are probably not technical but relate to the adverse economic environment of the early 1930s.

The Boxplane

Turning now to configurations related to the joined wing that have been wind tunnel-tested but not flown full-scale, mention must be made of the boxplane concept invented by Luis Miranda of Lockheed Corporation. Figure 41 illustrates a boxplane transport configuration studied by Lockheed.[35] Low-speed and transonic tests were also performed on a lower aspect-ratio boxplane representative of a fighter design.[36]

Compared to the joined wing, the boxplane differs in that the wings do not form a diamond shape in front view. An additional difference is that the boxplane internal wing structure does not follow the special form employed for the joined wing. The prime motivation of the boxplane was to obtain a high span-efficiency factor. Standard induced-drag theory predicts that, for a given height and span, the boxplane arrangement achieves the maximum possible span-efficiency factor. For example, Ref. 36 shows that with a height/span ratio of 0.3, the boxplane produces only 60% of the induced drag of an elliptic monoplane wing of the same span, operating at the same airspeed and air density and generating the same lift as the total lift of the front plus rear wings of the boxplane.

The low-speed wind tunnel tests verified the predicted savings of induced drag, but the transonic tests and the transport design studies uncovered some problems that led to the abandonment of U.S. Government sponsorship of boxplane research. The transport design studies revealed an unacceptably low flutter speed and also showed no saving in wing-plus-tail weight relative to a baseline conventional configuration. The transonic tests showed several problems, discussed below. These included high minimum drag coefficient and premature separation on the front wing at subsonic Mach numbers, leading to an increase in lift-dependent drag and lower maximum lift coefficient than that of a reference conventional configuration. With the benefit of hindsight, it appears that at least some of the aerodynamic problems noted in Ref. 36 could have been overcome, as discussed below.

There were three causes of the apparently disappointing results of the Ref. 36 boxplane tests. First, the airfoils of the boxplane were not designed with consideration to the flow curvature induced by the neighboring airfoil. Instead, standard monoplane airfoils were chosen. As was later shown by Addoms,[37] biplane configurations must employ airfoils having substantially different camber from those of competitive monoplanes. A fair comparison between monoplanes and multiwing configurations cannot be obtained if all the configurations are forced to use the same airfoils. As noted by Addoms, typically the use of monoplane airfoils on biplanes causes premature separation and unnecessarily low maximum lift.

The importance of the above point cannot be overstated for configurations such as boxplanes and joined wings. The use of "off-the-shelf" monoplane airfoils for such configurations is disadvantageous and is no longer necessary in view of the current state of airfoil design technology.

The second cause of the apparently disappointing performance of the boxplane in the tests of Ref. 36 was improper selection of reference areas. The reference area for the boxplane model was selected to be the same as that for the reference baseline model of conventional wing-plus-tail layout. The latter had 20% more total horizontal lifting surface area (due to its tail, which was not included in the reference area). Hence, the monoplane would be expected to produce a higher maximum lift coefficient because it has a higher ratio of lifting surface area to reference area. The third reason for the poor showing of the boxplane vs the monoplane in the tests of Ref. 36 was that the data were not corrected to full-scale Reynolds numbers. Although at $M=0.5$ the boxplane had a trimmed maximum L/D of 12.2 vs 11.1 for the conventional configuration trimmed at a dimensionally equal static margin, this result is less favorable than would be achieved at full-scale conditions. This is because, at model test Reynolds numbers, the short chord lengths of the boxplane wing increase its minimum drag over that of the reference monoplane by a larger proportion than at full scale.

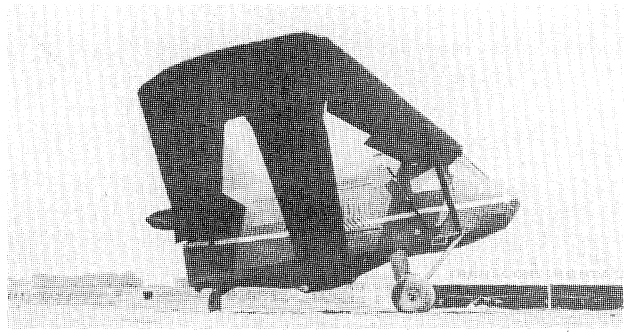

Fig. 40 1932 Brown airplane.

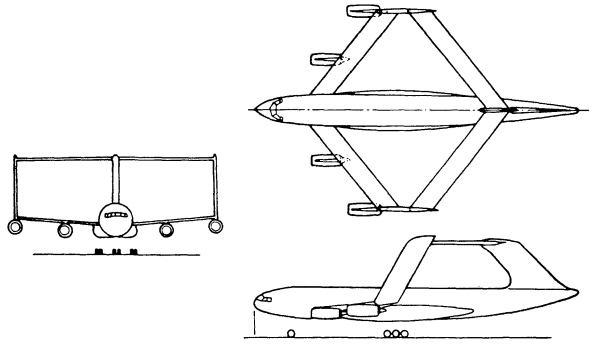

Fig. 41 Lockheed boxplane transport design.

In summary, the aerodynamic problems of the boxplane may be less severe than has been believed, and may be partly curable with proper airfoil design. The low Reynolds numbers of its short-chord wings may be acceptable for laminar flow airfoils. Low flutter speed and lack of weight saving are probably more serious drawbacks to the boxplane than any aerodynamic factors.

Other Concepts

A brief summary of other connected-wing concepts that are of research interest is given below.

Henderson and Huffman[38] present low-speed test data on a modified boxplane in which the rear wing root is mounted on top of the fuselage. Rhodes and Selberg,[39] Cahill and Stead,[40] and Zimmer[41] describe configurations in which a swept-back wing is connected at its tips to a second wing that is either swept forward or less highly swept-back than the first wing. Other examples of this category are the Warren-Young rhomboidal wing designs.[32] For all these configurations, the root of the front wing is higher than the root of the rear wing, and the fin is not directly connected to the rear wing. In these and other respects, the above configurations differ from the joined wing.

The wind tunnel models tested by Cahill and Stead were unsophisticated in some respects (one had flat-plate airfoils) and, as a result, had high induced drag. The Zimmer configuration was more refined but retained a separate horizontal and vertical tail, which did not connect with its front or rear wings. The Warren-Young, Cahill, Henderson, and Zimmer concepts do not detail any internal wing structure

comparable with that of the joined wing. Numerous other concepts have been proposed from time to time (e.g., the "ring wing," which forms a circle in front view and a parallelogram in side view), but data on these related configurations are fragmentary and incomplete, and their resemblances to the joined wing are less significant than their differences.

Acknowledgments

Part of the work reported herein was performed under NASA Contracts NAS2-11255 and NAS2-11725 and also under Navy Contracts N00014-79-C-0953 and N00014-82-C-0607. NASA Project Monitors were Mr. Thomas J. Gregory and Mr. George H. Kidwell. The Navy Project Monitor was Dr. Robert E. Whitehead.

References

[1]Wolkovitch, J., "Application of the Joined Wing to Cruise Missiles," Phase I, ONR-CR-212-266-1, Nov. 1980.

[2]Wolkovitch, J., Joined Wing Aircraft, U.S. Patent 3,942,747, March 1976.

[3]Wolkovitch, J., Joined Wing Aircraft, U.S. Patent 4,365,773, Dec. 1982.

[4]Clyde, J.A., "Transonic Design and Wind Tunnel Testing of a Joined Wing Concept," AIAA Paper 84-2433, 1984.

[5]Wolkovitch, J. and Bettes, W.H., "Low-Speed Wind Tunnel Test on Joined Wing and Monoplane Configurations, Vol. I: Analysis of Results, Vol. II: Test Data," ACA Industries, Inc., Rancho Palos Verdes, CA, ACA Report 82-2, 1984.

[6]White, E.R., "Preliminary Force Test Data for a Joined Wing Aircraft Configuration," NASA Langley Research Center, Hampton, VA, Internal Memo File V-19100/OLTR-094, April 8, 1980.

[7]Samuels, M.F., "Structural Weight Comparison of a Joined Wing and a Conventional Wing," *Journal of Aircraft*, Vol. 19, June 1982, pp. 485-491.

[8]Shyu, A., "Analysis of Structural Weights of Joined and Cantilever Wing Systems for Transports," forthcoming NASA Ames Research Center Report.

[9]Miura, H., Shyu, A., and Wolkovitch, J., "Parametric Weight Evaluation of Joined Wings by Structural Optimization," AIAA Paper 85-0642-CP, April 1985.

[10]Wolkovitch, J. and Lund, D.W., "Application of the Joined Wing to Turboprop Transport Aircraft," forthcoming NASA CR-22187.

[11]Hajela, P., "Weight Evaluation of the Joined Wing Configuration," Final Report, Department of Engineering Sciences, University of Florida, Gainesville, FL, 1983.

[12]Turner, C.D. and Ricketts, R.H., "Aeroelastic Considerations for Patrol High Altitude Surveillance Platforms," AIAA Paper 83-0924-CP, 1983.

[13]Durham, M.H., "Flutter Tests on High-Aspect-Ratio Model Joined and Cantilever Wings for High Altitude Platforms," Kentron International Corp., Hampton, VA.

[14]Jones, R.T., "Classical Aerodynamic Theory," NASA Reference Publication 1050, 1979.

[15]Letcher, J.S., "V-Wings and Diamond-Ring Wings of Minimum Induced Drag," *Journal of Aircraft*, Vol. 9, Aug. 1972, pp. 605-607.

[16]Kulhman, J.M. and Ku, T.J., "Numerical Optimization Techniques for Bound Circulation Distribution for Minimum Induced Drag of Non-Planar Wings: Computer Program Documentation," NASA CR-3458, 1982.

[17]Wolkovitch, J., "Subsonic VSTOL Aircraft Configurations with Tandem Wings," *Journal of Aircraft*, Vol. 16, Sept. 1979, pp. 605-611.

[18]Igoe, W.B., Re, R.J., and Cassetti, M.D., "Transonic Aerodynamic Characteristics of a Wing-Body Combination Having a 52.5 Deg Sweptback Wing of Aspect Ratio 3 and Conical Camber and Designed for a Mach Number of $\sqrt{2}$," NASA TN D-817, May 1961.

[19]DeLaurier, J., "Drag of Wings with Cambered Airfoils and Partial Leading-Edge Suction," *Journal of Aircraft*, Vol. 20, Oct. 1983, pp. 882-886.

[20]Addoms, R.B. and Spaid, F.W., "Aerodynamic Design of High Performance Biplane Wings," *Journal of Aircraft*, Vol. 12, Aug. 1975, pp. 629-630.

[21]Clyde, J.A., Bonner, E., Goebel, T.P., and Spacht, L., "Joined Wing Transonic Design and Test Validation," Rockwell International Corp., NAAO Div., Los Angeles, CA, Rept. 84-1434, June 1984.

[22]Lamar, J.E., "A Vortex-Lattice Method for the Mean Camber Shapes of Trimmed Noncoplanar Planforms with Minimum Vortex Drag," NASA TN D-8090, 1976.

[23]White, E.R., "Low-Speed Wind-Tunnel Investigation of a Joined-Wing Aircraft Configuration," forthcoming NASA Report.

[24]Hoerner, S.F. and Borst, H.V., "Fluid-Dynamic Lift," Hoerner Fluid Dynamics, Brick Town, NY, 1975.

[25]Wolkovitch, J., "Joined-Wing Research Airplane Feasibility Study," AIAA Paper 84-2471, 1984.

[26]Bulot, C., "Joined Wings: Modernizing an Old Concept," *Homebuilt Aircraft*, Vol. 10, March 1983, pp. 20-23, and 70.

[27]Levy, H., "Oshkosh 84," *Flight International* (U.K.), Sept. 15, 1984, pp. 680-681.

[28]"Microlights Join Together," *Flight International* (U.K.), Nov. 10, 1984, pp. 1237.

[29]"Trident T 3 Brochure," Summit Aircraft Corp., Denton, TX.

[30]Goldsmith, I.M., "A Study to Define the Research and Technology Requirements for Advanced Turbo/Propfan Transport Aircraft," Douglas Aircraft Company, Long Beach, CA, NASA CR-166138, 1981.

[31]"An Original All-British Aeroplane," *Flight*, (U.K.), Feb. 5, 1910, pp. 87-90.

[32]Hall-Warren, N., "Design of Tailless Aircraft," *Flight* (U.K.), Aug. 10, 1950, pp. 179-181.

[33]Platz, R., "Ein neuartiges Segelflugzeug," *Zeitschrift fur Flugtechnik und Motor Luftschiffahrt*, Vol. 13, 1922.

[34]Bowers, P.M., *Unconventional Aircraft*, Tab Books, Inc., Blue Ridge Summit, PA, 1984.

[35]Lange, R.H. et al., "Feasibility Study of the Transonic Biplane Concept for Transport Aircraft Application," NASA CR-132462, 1974.

[36]Miranda, L.R. and Dougherty, G.L., "Transonic Wind Tunnel Testing of a Low Induced Drag Lifting System, Vols. I and II," Lockheed Aircraft Corp., Burbank, CA, Feb. 1974.

[37]Addoms, R.B. and Spaid, F.W., "Aerodynamic Design of High Performance Biplane Wings," *Journal of Aircraft*, Vol. 12, Aug. 1975, pp. 629-630.

[38]Henderson, W.P. and Huffman, J.K., "Aerodynamic Characteristics of a Tandem Wing Configuration at a Mach Number of 0.30," NASA TM X-72779, Oct. 1975.

[39]Rhodes, M.D. and Selberg, B.P., "Benefits of Dual Wings over Single Wings for High-Performance Business Airplanes," *Journal of Aircraft*, Vol. 21, Feb. 1984, pp. 116-127.

[40]Cahill, J.F. and Stead, D.H., "Preliminary Investigation at Subsonic and Transonic Speeds of Aerodynamic Characteristics of a Biplane Composed of a Swept-Back and Swept-Forward Wing Joined at the Tip," NACA RM L53L34B, March 1954.

[41]Zimmer, H., "Das Hochauftribsverhalten beim Rautenflugelkonzept," Dornier GMBH, Friedrichshafen, Germany, DGLR Rept. No. 78-114, 1978.